J. Fluid Mech. (1990), *vol.* 217, *pp.* 487–518
Printed in Great Britain

Dynamical behaviour of natural convection in a single-phase loop

By PETER EHRHARD AND ULRICH MÜLLER
Kernforschungszentrum Karlsruhe, Institut für Reaktorbauelemente, Postfach 3640, D-7500 Karlsruhe, FRG

(Received 31 January 1989 and in revised form 4 January 1990)

A one-dimensional model is derived for natural convection in a closed loop. The physical model can be reduced to a set of nonlinear ordinary differential equations of the Lorenz type. The model is based on a realistic heat transfer law and also accounts for a non-symmetric arrangement of heat sources and sinks. A nonlinear analysis of these equations is performed as well as experiments to validate the model predictions.

Both the experimental and the analytical data show that natural convection in a loop is characterized by strong nonlinear effects. Distinct subcritical regions are observed in addition to a variety of stable steady flow regimes. Thus, in certain ranges of the forcing parameter the flow stability depends significantly on the presence of finite perturbation amplitudes. An absolutely unstable range also exists which is characterized by a chaotic time behaviour of the flow quantities. It is also shown that the steady solutions are subject to an imperfect forward bifurcation if heating of the loop is performed non-symmetrically. In such a case one flow direction is preferred at the onset of convection and, moreover, the corresponding steady solution is more stable than a second, isolated, steady solution. The second solution has the opposite flow direction and is stable only in a relatively small, isolated interval. The preferred steady solution becomes unstable against time-periodic perturbations at a higher value of the forcing parameter. A backward- or a forward-directed bifurcation of the periodic solutions is found depending on the non-symmetry parameter of the system.

1. Introduction

Natural convection in closed loops sometimes plays an important role in the design of thermal energy systems, such as solar heating systems and nuclear reactors. The configurations of these systems are characterized by an arrangement of a heat source together with one, or several, heat sinks positioned at some height above the heat source. These components are usually connected by pipes forming at least one closed loop. Reviews of natural circulation loops in engineering systems have been given by Zvirin (1981), Mertol & Greif (1984), and most recently by Greif (1988).

Natural circulation in a single loop has been investigated previously by several authors, with the main motivation being the fundamental study of simple systems exhibiting typical nonlinear convective effects (see e.g. Welander 1967 and Creveling *et al.* 1975). Malkus (1972) and Yorke & Yorke (1981) have proposed a model in which they represent the physics of a symmetrically heated loop using a set of three ordinary differential equations of the Lorenz type (see Lorenz 1963). Although various authors have developed models for fully turbulent flow in such geometries

using appropriate friction and heat transfer correlations (see e.g. Creveling *et al.* 1975; Hart 1984; Widmann, Gorman & Robins 1989), realistic modelling of the heat transfer in the laminar flow regime is still lacking. Recently Yorke, Yorke & Mallet-Paret (1987) have presented an approach based on a two-dimensional model. In particular they retain radial diffusion terms in both the momentum and the heat transport equation, whereas the wall temperature distribution is stipulated.

A detailed nonlinear analysis on the effect of non-symmetric heating of the loop has not yet been performed: Hart (1984) does consider it briefly. He calculates the steady convective solutions for different values of a non-symmetry parameter, determines the linear stability of these solutions, and presents some preliminary results concerning the nonlinear dynamics of the system. A first experimental investigation on the effect of non-symmetric heating has been conducted by Damerell & Schoenhals (1979), who presented results on the stability of the preferred steady flow.

In addition to the convective flow in a single loop, a system of two coupled loops have been considered recently by several authors. Davis & Roppo (1987) have investigated theoretically the stability of the flow in two thermally coupled loops, while Ehrhard, Karcher & Müller (1989) also incorporated momentum exchange and carried out complementary experiments.

In this work we extend the model for the flow in a single loop used by Yorke & Yorke (1981) to conditions of non-symmetric heating, as well as to a more realistic heat transfer situation. We perform this investigation by applying analytical and numerical mathematical methods to the model equations. In parallel to the theoretical investigation, an experimental programme has been undertaken in which temperatures and velocities have been measured for comparison with the theoretical results.

Figure 1 shows schematically the experimental set-up and illustrates the problem. We consider a circular loop filled with an incompressible fluid. The cross-section A of the tube is circular and constant. The lower semicircle of the loop is heated by circulating coolant at a temperature T_H through a jacket surrounding the tube, while the upper semicircle is cooled by connecting a corresponding jacket to a water bath at a lower temperature T_C. The temperature distribution at the tube wall is represented by the function $T_W(\varphi)$, where φ is the toroidal coordinate. We also allow for an offsetting of the heating and cooling zones by an angle, δ, relative to the symmetric position. The symmetric position, i.e. $\delta = 0$, is therefore characterized by imposing a high wall temperature T_H in the region $-\frac{1}{2}\pi < \varphi < \frac{1}{2}\pi$ and a low wall temperature T_C in the region $\frac{1}{2}\pi < \varphi < \frac{3}{2}\pi$.

If we increase the forcing temperature difference $\Delta T = T_H - T_C$ in a symmetrically heated system beyond a certain threshold value, the initial state of heat conduction is replaced by a convective flow in either the positive or the negative φ-direction. For a temperature difference ΔT well above this first critical value, the steady-state convection becomes unstable and is replaced by a time-dependent flow. Moreover, it is evident that non-symmetric heating induces a preferred flow direction. Crucial questions arising in this context are: What are the boundaries of stability of the steady convection with respect to infinitesimally small or finite-amplitude perturbations? What are the particular features of steady and unsteady flow with respect to the present parameters?

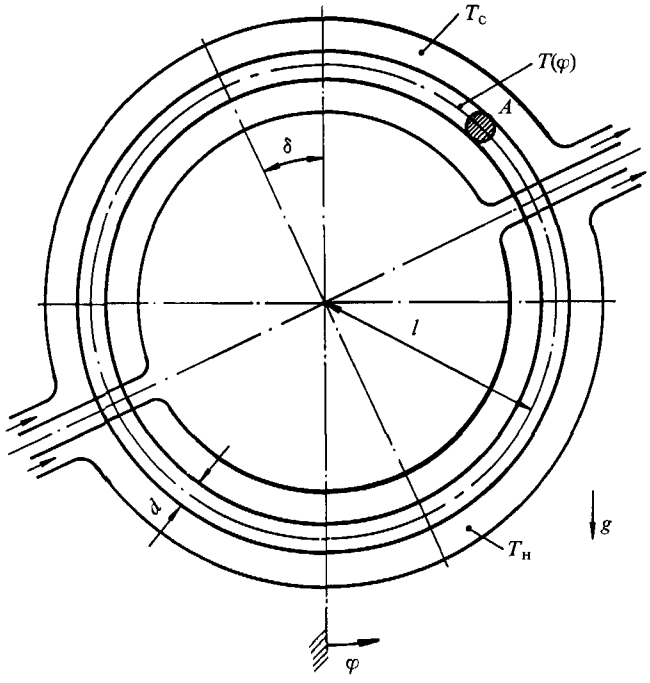

FIGURE 1. Principle sketch of a loop with imposed wall temperatures.

2. Theory

2.1. *Model equations*

Assuming the internal diameter of the loop pipe to be much smaller than its length, i.e. $d \ll l$, a one-dimensional modelling of the flow and heat transfer processes proves to be of sufficient accuracy (cf. Welander 1967; Yorke & Yorke 1981). Using the Boussinesq approximation we obtain for the cross-sectionally averaged velocity $u(t)$, pressure $p(\varphi, t)$ and temperature $T(\varphi, t)$ in the loop the following set of partial differential equations:

$$\left.\begin{aligned} &\frac{\partial u}{l\,\partial\varphi} = 0, \quad \rho_0 \frac{\partial u}{\partial t} = -\frac{\partial p}{l\,\partial\varphi} - \rho(T)\, g \sin(\varphi) - f_W, \\ &\rho_0 c_p \left\{\frac{\partial T}{\partial t} + u \frac{\partial T}{l\,\partial\varphi}\right\} - \lambda \frac{\partial^2 T}{l^2\,\partial\varphi^2} = h_W[T_W(\varphi) - T] + q_W(\varphi) \end{aligned}\right\} \tag{1}$$

As a consequence of using a one-dimensional model, the equations (1) do not involve velocity and temperature gradients in the cross-section A of the pipe. For this reason we have to introduce closure conditions into the mathematical model for the interaction of the fluid with the wall. The corresponding terms in (1) are denoted by f_W, h_W and q_W.

Here f_W represents the friction force due to the velocity gradient at the wall. Estimates, based on the stability of the flow in a straight circular tube under isothermal conditions, show that laminar flow exists for our geometry conditions and test fluid, i.e. water. For this reason it is appropriate to use a linear correlation between the friction term f_W and the velocity u:

$$f_W = \tfrac{1}{2}\rho_0 f_{W0}\, u. \tag{2}$$

We also require a correlation for the heat transfer coefficient at the wall h_W. It is known from measurements in straight circular tubes that h_W is constant for small values of u, but varies as $h_W \propto |u|^{\frac{1}{3}}$ for moderate values of u in the laminar flow regime (see e.g. Schlünder 1981) Thus we later introduce into the analysis an asymptotic model equation reflecting this behaviour (see (6)). We also demonstrate the validity of the above correlations for f_W and h_W in the actual test apparatus (see §3.2).

The right-hand side of the heat transport equation in (1) represents source terms. In addition to a heat flux due to the temperature difference $\{T_W(\varphi) - T\}$, a volumetric heat source $q_W(\varphi)$ may be taken into account.

By introducing Fourier series for the φ-dependent functions and using a Galerkin method, the partial differential equations are transformed into an infinite number of ordinary differential equations. In detail we use the expansions

$$\left.\begin{aligned} T(\varphi, t) &= T_0(t) + \sum_{n=1}^{\infty} \{S_n(t) \sin(n\varphi) + C_n(t) \cos(n\varphi)\}, \\ Q(\varphi) &= Q_0 + \sum_{n=1}^{\infty} \{Q_n \sin(n\varphi) + R_n \cos(n\varphi)\} \end{aligned}\right\} \tag{3}$$

for the temperature distribution $T(\varphi, t)$ inside the loop and the source term $Q(\varphi)$ in the heat transport equation, where

$$Q(\varphi) = \frac{1}{\rho_0 c_p} \{h_W T_W(\varphi) + q_W(\varphi)\}. \tag{4}$$

We introduce the dimensionless variables of state x_i and time t' as

$$\left.\begin{aligned} t' &= \frac{h_{W0}}{\rho_0 c_p} t, \quad x_1 = \frac{\rho_0 c_p}{l h_{W0}} u, \quad x_0 = \frac{\rho_0 c_p}{h_{W0}} \frac{\gamma g}{f_{W0} l} T_0, \\ x_2 &= \frac{\rho_0 c_p}{h_{W0}} \frac{\gamma g}{f_{W0} l} S_1, \quad x_3 = \frac{\rho_0 c_p}{h_{W0}} \frac{\gamma g}{f_{W0} l} \left\{\frac{\rho_0 c_p}{h_{W0}} R_1 - C_1\right\}, \\ x_{2n} &= \frac{\rho_0 c_p}{h_{W0}} \frac{\gamma g}{f_{W0} l} S_n, \quad x_{2n+1} = \frac{\rho_0 c_p}{h_{W0}} \frac{\gamma g}{f_{W0} l} C_n, \end{aligned}\right\} \tag{5}$$

where γ is the coefficient of thermal expansion, c_p the specific heat, ρ_0 the reference density, λ the heat conductivity and g the acceleration due to gravity. Furthermore, we use the following constitutive relation (see e.g. Schlünder 1981) for the heat transfer:

$$h_W = h_{W0}\{1 + K|x_1|^{\frac{1}{3}}\}. \tag{6}$$

As a result we obtain a set of coupled ordinary differential equations in time for the velocity x_1 and the coefficients of the temperature distribution $(x_2, x_3, \ldots)$ in the loop

$$\left.\begin{aligned} \dot{x}_1 &= \alpha[x_2 - x_1], \\ \dot{x}_2 &= \beta x_1 - x_2\left[1 + K|x_1|^{\frac{1}{3}} + \frac{\lambda}{l^2 h_{W0}}\right] - x_1 x_3 + \beta \tan\delta, \\ \dot{x}_3 &= x_1 x_2 - x_3\left[1 + K|x_1|^{\frac{1}{3}} + \frac{\lambda}{l^2 h_{W0}}\right]; \end{aligned}\right\} \tag{7a}$$

and for $n \geqslant 2$

$$\left.\begin{aligned} \dot{x}_{2n} &= nx_1 x_{(2n+1)} - x_{2n}\left[1 + K|x_1|^{\frac{1}{3}} + \frac{n^2\lambda}{l^2 h_{\mathrm{W}0}}\right] + \beta'_n, \\ \dot{x}_{(2n+1)} &= -nx_1 x_{2n} - x_{(2n+1)}\left[1 + K|x_1|^{\frac{1}{3}} + \frac{n^2\lambda}{l^2 h_{\mathrm{W}0}}\right] + \beta_n. \end{aligned}\right\} \tag{7b}$$

To be complete we finally give the zero-order equation

$$\dot{x}_0 = \beta_0 - x_0, \tag{7c}$$

which describes the mean temperature in the loop, x_0, established via a vanishing exponential function. For all further experimental and analytical procedures x_0 is assumed to be already steady, i.e.

$$x_0 = \beta_0 = \frac{\gamma g}{f_{\mathrm{W}0} l}\left\{\frac{\rho_0 c_p}{h_{\mathrm{W}0}}\right\}^2 Q_0.$$

In (7*a–c*) $\dot{x}_i$ denotes the derivative of x_i with respect to t'.

There are five dimensionless groups in (7*a*, *b*). The fluid/wall parameter α relates the wall friction coefficient to the heat transfer coefficient at the wall:

$$\alpha = \frac{1}{2}\frac{\rho_0 c_p}{h_{\mathrm{W}0}} f_{\mathrm{W}0}.$$

To a certain extent this group is comparable to the Prandtl number in ordinary viscous flow and depends on the transport coefficients for heat and momentum $f_{\mathrm{W}0}, h_{\mathrm{W}0}$ and the fluid properties ρ_0, c_p. The heating rate β represents the balance between work of buoyancy forces and overall losses of energy, caused by losses of heat and momentum:

$$\beta = \frac{\gamma g}{f_{\mathrm{W}0} l}\left(\frac{\rho_0 c_p}{h_{\mathrm{W}0}}\right)^2 R_1.$$

This parameter is directly proportional to the forcing temperature difference ΔT and comparable to the Rayleigh number in the Bénard convection problem. The angle δ relates the odd modes of the source term $Q(\varphi)$ to the even modes:

$$\delta = \arctan\left(\frac{Q_1}{R_1}\right).$$

This relation characterizes the symmetry of the heat transfer to and from the loop. The group $\lambda/(l^2 h_{\mathrm{W}0})$ accounts for the influence of the heat conduction within the fluid. It can be shown that, because $\lambda/(l^2 h_{\mathrm{W}0}) \ll 1$, this contribution to the overall heat transport along the φ-direction may be neglected even for media with low Prandtl numbers. This result is equivalent to the approximation made by other authors who neglect the conduction term in the basic heat transport equation and assume that convection dominates (see e.g. Welander 1967; Creveling *et al.* 1975). The nonlinear closure condition for the heat transfer coefficient $h_{\mathrm{W}}(u)$, equation (6), is characterized by a constant K, which may be determined experimentally. In the higher-order equations (7*b*), the contribution of the source term $Q(\varphi)$ (see equation (3)) due to the Fourier mode n is given by the dimensionless groups

$$\beta'_n = \frac{\gamma g}{f_{\mathrm{W}0} l}\left(\frac{\rho_0 c_p}{h_{\mathrm{W}0}}\right)^2 Q_n \quad \text{and} \quad \beta_n = \frac{\gamma g}{f_{\mathrm{W}0} l}\left(\frac{\rho_0 c_p}{h_{\mathrm{W}0}}\right)^2 R_n.$$

On examining the structure of (7*a*, *b*) we see that the motion of the fluid, described

by the velocity amplitude x_1, is related only to the first mode of the temperature distribution characterized by x_2 and x_3. Thus, the first three nonlinear equations (7*a*) can be solved separately, and these completely determine the structure of the solutions. However, if a more detailed temperature distribution is required, the higher-mode equations (7*b*) must be solved. Knowing the solutions for x_1, x_2, x_3, the differential equations for the higher-order amplitudes x_{2n} and x_{2n+1}, $n \geqslant 2$, are linear and can be solved successively. The decoupling of the first three equations (7*a*) has also been noted by Yorke & Yorke (1981). Likewise, Hart (1984) separated the problem into a so-called master problem for the first basic mode and adjacent slave problems for the higher-temperature modes. If we neglect the heat conduction in the direction of the tube axis then we have to solve the following equations:

$$\left.\begin{aligned} \dot{x}_1 &= \alpha[x_2 - x_1], \\ \dot{x}_2 &= \beta x_1 - x_2[1 + K|x_1|^{\frac{1}{3}}] - x_1 x_3 + \beta \tan\delta, \\ \dot{x}_3 &= x_1 x_2 - x_3[1 + K|x_1|^{\frac{1}{3}}], \end{aligned}\right\} \tag{8}$$

in order to obtain the velocity amplitude x_1.

For the case of symmetric heating with $\delta = 0$ and constant heat transfer coefficient, i.e. $K = 0$, the above system of equations (8) is identical with the Lorenz equations, which approximately describe convection in a horizontal liquid layer heated from below and cooled from above (Lorenz 1963).

2.2. *Solution procedure*

We first determine steady solutions $\boldsymbol{x}_{\mathrm{st}}$ to (8) and then we investigate their stability. In order to do this, we introduce small time-dependent perturbations into the system of the form

$$\boldsymbol{x}(t') = \boldsymbol{x}_{\mathrm{st}} + \delta\boldsymbol{x}_{\mathrm{st}}(t'), \tag{9}$$

with $|\delta\boldsymbol{x}_{\mathrm{st}}| \ll 1$, and linearize in $\delta\boldsymbol{x}_{\mathrm{st}}$. On introducing exponential functions for the time-dependent variables in the form $\delta\boldsymbol{x}_{\mathrm{st}} \propto \exp(\sigma t')$, we obtain an eigenvalue problem for the amplitudes of the disturbances, with the temporal amplification rates σ as the eigenvalues. By computing the eigenvalues, conclusions can be drawn concerning the stability bounds of all the different steady states.

Naturally, the nonlinear properties of (8) cannot be revealed by this linearizing procedure. The presence of finite-amplitude disturbances requires the solution to the fully nonlinear equations. The complete set of periodic solutions is obtained numerically by using a multiple shooting method. We solve the related boundary-value problem for (8) which results from applying the periodicity condition

$$\boldsymbol{x}_{\mathrm{p}}(t') = \boldsymbol{x}_{\mathrm{p}}(t' + \tau), \tag{10}$$

where τ is the time period of oscillation. The numerical procedure starts with an estimated set of solutions and shooting parameter τ and then solves iteratively the fully nonlinear equations (8) in the interval $0 \leqslant t' \leqslant \tau$, subject to the given boundary conditions (10). We keep the parameters $(\alpha, \beta, \delta, K)$ fixed while solving the boundary-value problem. For a discrete value of τ solutions may be found. Then a continuation algorithm traces the solutions using the computed solutions and shooting parameter τ as new estimates for the next adjacent calculation, i.e. at a slightly varied set of parameters $\{\alpha, \beta, \delta, K\}$. With this method the nonlinear solutions are computed effectively for varied parameters; in particular, the results presented below are computed for varied β. The basic idea of this solution procedure has been suggested by Kubiček & Marek (1983).

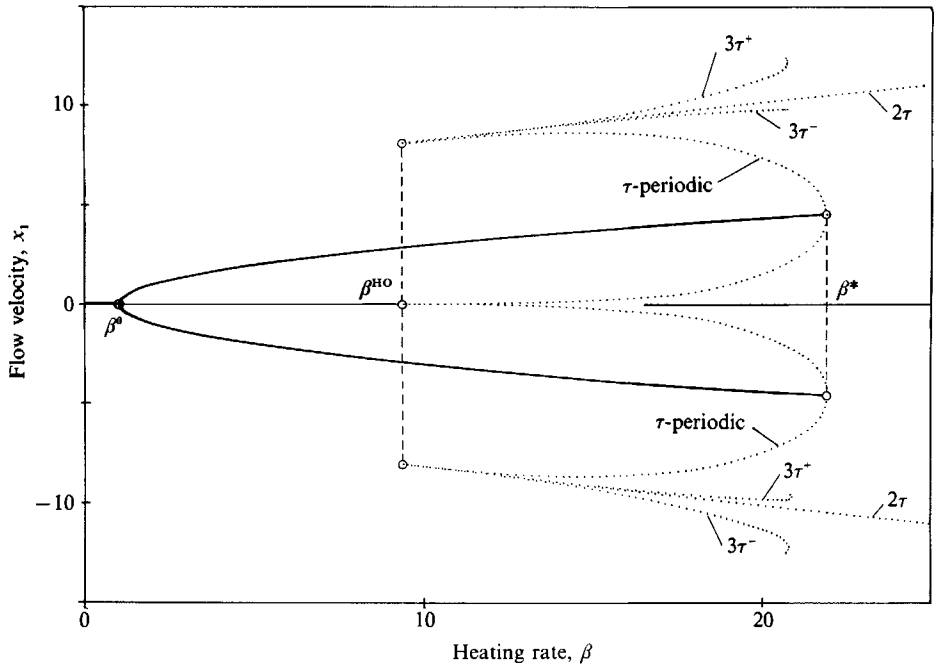

FIGURE 2. Bifurcation diagram for symmetric heating in terms of the velocity in the loop ($\alpha = 15$, $\delta = 0, K = 0$); solid lines represent stable steady branches, ○ mark stability bounds, dotted lines give amplitudes of periodic solutions.

In detail, we use a multiple shooting algorithm to solve the boundary-value problem, which employs a fourth-order Runge–Kutta integration procedure. In the continuation algorithm, in order to trace the calculated solution branches, a Fourier series representation of the nonlinear periodic solutions of 64th order is employed.

Having determined these solutions we perform a linear stability analysis by imposing small perturbations on the periodic orbit. We evaluate the conditions of stability for the periodic solutions with the aid of Floquet's theory (see e.g. Joseph 1976). This is done by calculating the Floquet multipliers numerically, since the nonlinear solutions have no analytical representation. Therefore a numerical integration procedure (fourth-order Runge–Kutta) is again employed to compute the monodromy matrix.

2.3. *Results for symmetric heating*

Although there is a vast amount of literature on the properties of the solution of the symmetric Lorenz equations (see e.g. Sparrow 1982), we present here solutions for a set of parameters appropriate for a comparison with our experimental results reported in §3.3. We obtain solutions for the case of symmetric heating by setting $\delta = 0$ in the model equations (8) and using the solution procedure outlined in §2.2. The results are compiled in figure 2, where the flow velocity, x_1, is plotted versus the heating rate β. For reason of clarity the numerical solutions are presented here in a comprehensive way only for a constant heat transfer coefficient $h_W\,(K = 0)$ and a constant fluid/wall parameter $\alpha = 15$. The influences of a more realistic heat transfer law, (6) and $K \neq 0$, and variable α are discussed in detail in §2.5. Results for the data set $\alpha = 15, K = 0.35$, relevant for our experiment, are used for the comparison between experiment and theory in §3.3.

Starting from the isothermal situation, corresponding to $\beta = 0$, we find for low

values of β only the zero solution, i.e. the state of rest. At $\beta = \beta^0 = 1$ two convective solutions branch off symmetrically from the zero solution in the direction of increasing β. This type of branching is usually termed a perfect forward, or pitchfork bifurcation. Thus, in the range $0 \leqslant \beta \leqslant \beta^0$ the model equations (8) possess a solution without motion. We call this a 'conductive solution', since physically heat is transported only by diffusion, although this mechanism is not included in the model. The forward bifurcation at $\beta = \beta^0$ implies the loss of stability for the conductive solution with velocity amplitude $x_1 = 0$, and the emergence of two stable convective solutions for $\beta > \beta^0$ with flow in either the clockwise or counterclockwise direction.

If the heating rate β is increased further we find that at $\beta^* = 21.92$ these steady solutions become unstable with respect to oscillatory disturbances. At this stability bound periodic solutions branch off from the steady solutions. We call this particular branching point a Hopf bifurcation point or in short a Hopf point (see Hopf 1942).

We find from a nonlinear stability analysis (Ehrhard 1988; see also McLaughlin & Martin 1975) as well as from direct numerical evaluation of (8) that the τ-periodic solutions have growing amplitudes for decreasing values of the heating rate β starting from β^*, i.e. the bifurcation is backward. A so-called homoclinic orbit occurs for a value $\beta^{HO} = 9.4$. For this particular heating rate the amplitude of the respective periodic solution approaches the value $\boldsymbol{x} = 0$ of the stationary unstable conductive solution. As the value β^{HO} of the periodic solution is approached from values $\beta > \beta^{HO}$, the period of oscillation tends to infinity. Owing to the symmetry of the τ-periodic solutions the above phenomena occur simultaneously at both τ-periodic orbits. This configuration and its structural implications are commonly denoted as a homoclinic bifurcation point or homoclinic explosion (see Sparrow 1982 or Guckenheimer & Holmes 1983). It turns out that embedded in a 'strange invariant set' of solutions a countable infinite number of subharmonic periodic solutions originate from this homoclinic bifurcation point. They exist for increasing values of the heating rate β. We have calculated the periodic solutions up to the order 8τ. To allow a clear presentation only the calculated solutions of lower order, denoted by τ, 2τ, $3\tau^+$ and $3\tau^-$, are given in figure 2. While the 2τ-periodic solution proves to be symmetric with respect to the $x_1 = 0$ line, $3\tau^+$ and $3\tau^-$ denote two different mirror-symmetric 3τ-periodic solutions. The 3τ-periodic solutions are found to disappear as the heating rate β increases prior to the Hopf point, i.e. for a value $\beta < \beta^*$. This can be seen in figure 2. Employing Floquet's theory we find that the computed periodic solutions are locally unstable in the investigated parameter range.

Our findings concerning the set of unstable periodic orbits existing to the right of the homoclinic bifurcation point, i.e. for values $\beta > \beta^{HO}$, as well as the disappearance of periodic orbits as the control parameter β is increased, are consistent with results of several authors, who employed direct numerical integration and different parameter sets of the Lorenz system. Namely Robbins (1977) and Sparrow (1982) present results for the sets $(\alpha = 5, b = 1)$ and $(\alpha = 10, b = \frac{8}{3})$ while we use the set $(\alpha = 15, b = 1)$. In addition they infer the existence of an infinite set of unstable aperiodic orbits and an infinite set of trajectories terminating at $\boldsymbol{x} = 0$ within the strange invariant set. Together with the set of unstable periodic orbits these form a dense bundle of trajectories in the phase space, existing for values $\beta \geqslant \beta^{HO}$. Sparrow concludes that all these members of the strange invariant set are individually unstable in the sense of Liaponov in a certain parameter range $\beta^{HO} \leqslant \beta \leqslant \beta^*$. The above authors furthermore infer from their calculations that the strange invariant set becomes a 'strange attractor' for increasing values of β prior to the Hopf point, i.e. for some value $\beta \leqslant \beta^*$. As a consequence of those findings one would expect the

time behaviour of the system to be chaotic even in the limit $t \to \infty$ within this range, provided a finite-amplitude disturbance has forced the system to leave the vicinity of the steady flow. The strange attractor thus attracts and confines the system to a dense set of unstable states independent of the initial conditions. Holodniok, Kubiček & Marek (1982) have performed similar calculations by a numerical continuation method, but for the parameter set ($\alpha = 16, b = 4$). Their results on the set of periodic solutions are consistent with our results.

The awareness of these unstable periodic solutions and, moreover, of the complete strange invariant set in the neighbourhood of steady stable branches leads us to evaluate the system behaviour when finite-amplitude disturbances act on it. We use here the definitions of 'stability of solutions' according to Joseph (1976). The system is absolutely stable in the range $0 \leqslant \beta < \beta^0$, since only the stable conductive solution exists. Furthermore, we conclude that a conditionally stable steady flow occurs in the range $\beta^0 \leqslant \beta < \beta^{HO}$, since two stable steady convective solutions coexist in this range and a transition from one to the other may be induced by finite-amplitude disturbances. In the range $\beta^{HO} \leqslant \beta < \beta^*$ the time history of the flow can exhibit a more complex behaviour. In this range sufficiently small perturbations of the steady solutions will generally be damped away according to the predictions of a linear stability analysis. However, if a finite-amplitude disturbance exceeds a certain critical value a time-dependent flow will occur in the loop. This flow will generally exhibit irregular, so-called chaotic oscillations (see Sparrow 1982), which typically involve flow reversals. Therefore, in this range the steady solutions are, even individually, only conditionally stable. Here the onset of an unsteady flow induced by finite-amplitude disturbances is related to the backward-bifurcating unstable Hopf solution and to the unstable strange invariant set, involving the unstable $n\tau$-periodic solutions ($n \geqslant 2$). The steady solution is usually called subcritically unstable and the region where this occurs is termed the subcritical region. We shall call the temporal behaviour of the system in this region transient-chaotic following the terminology of Gorman, Widmann & Robbins (1986). This feature can be explained by the wandering of the solution on the strange invariant set, including the rare event of spiralling into the stable steady branch in the long term, i.e. in a strict mathematical sense, in the limit $t' \to \infty$. Following Robbins (1977) and Sparrow (1982) a strange attractor is formed when the duration of the chaotic wandering tends to infinity with increasing values of β. This is typically achieved, as outlined before, in a small range prior to the Hopf point, i.e. for a value $\beta < \beta^*$. Thus the subcritical region $\beta^{HO} < \beta < \beta^*$ may be subdivided, depending on whether or not the system will spiral into the locally stable steady solution in the limit $t \to \infty$.

A fully chaotic time behaviour of the convection is to be expected for the parameter range $\beta > \beta^*$ where, apart from the multiple unstable periodic and aperiodic solutions and the unstable steady solutions, the strange attractor is continued. As a consequence the physical system should exhibit chaotic velocity and temperature histories featuring flow reversals at irregular time intervals.

The above description of the stability behaviour of the system in various parameter ranges agrees largely with results of Robbins (1977), which Gorman *et al.* (1986) have compared with experimental results. Given our results on the set of multiple unstable periodic solutions and locally stable steady solutions in the subcritical range, i.e. $\beta^{HO} < \beta < \beta^*$, we are not able to provide information on whether the strange invariant set exhibits an attracting character within a small subregion. Sparrow (1982) suggests that the structure of the strange invariant set is changed by removing periodic or aperiodic orbits as the control parameter β

increases. In particular he associates the disappearance of periodic orbits with new 'homoclinic explosions'. One might therefore speculate whether the disappearance of the 3τ-periodic solutions as found prior to the Hopf point (see figure 2) indicates this change in the structure of the strange invariant set. Interesting though such questions might be mathematically, we consider the physical consequences in finite observation times and in real test facilities as practically identical. Therefore we do not subdivide the subcritical region when comparing our theoretical and experimental results. In contrast Robbins does so, calling the regions 'transient subcritical' and 'subcritical'. We compare the 'critical' values of β obtained by Robbins with our stability bounds in §4.

2.4. *Results for non-symmetric heating*

In this section we discuss the theoretical results for a non-symmetric arrangement of the heat sources and sinks. In this case we solve (8) for values $\delta \neq 0$. For reasons of simplicity we still assume $K = 0$ and keep α constant in order to deal with a one-parameter problem only. The results of the calculations are shown in figure 3 for two different angles of non-symmetry, $\delta = 5°$ and $\delta = 15°$.

There are two steady convective solutions shown in figures 3(a) and 3(b): as a result of the non-symmetry, convection exists for any $\beta \neq 0$. For $\delta > 0$ the fluid will preferentially circulate counterclockwise, i.e. in the positive φ-direction, since the corresponding solution branch varies continuously with increasing heating rate β, beginning at $\beta = 0$. We call this solution branch 'preferred'. Physically, the fluid is rising at the one-sided extended heated zone of the loop determined by the sign of δ. The steady solution describing clockwise convection, i.e. a flow in the negative φ-direction, is not connected to the preferred solution branch. This solution branch is called 'isolated'. In an experiment, or in a direct numerical simulation, this solution can only be obtained in a transient manner, for example by imposing large initial perturbations of the heating rate or the momentum on the system. The situation described above is usually termed an imperfect forward bifurcation of the basic state.

The two steady solutions lose their stability to infinitesimally small oscillatory perturbations for higher heating rates. The bounds of stability for the two steady convective solutions are different. The bound β_1^* of the isolated solution corresponds to a low heating rate, while the bound of the preferred solution β_2^* represents a considerably higher heating rate. The non-symmetry clearly causes a stabilization of the steady convection in the preferred direction.

The stability analysis for the steady solutions shows that the stability bounds β_1^* and β_2^* are bifurcation points for periodic solutions, i.e. Hopf points. A nonlinear stability analysis in the vicinity of the Hopf points (see Ehrhard 1988) and the direct numerical evaluation of the nonlinear system (8) both show that the periodic solutions may branch off from the preferred steady solution in forward or backward directions, depending on the size of the non-symmetry parameter δ. In contrast, we find that a backward bifurcation of the periodic solution always occurs on the isolated branch of the steady solutions. These features are demonstrated in figure 3(a) with $\delta = 5°$ and figure 3(b) with $\delta = 15°$.

The numerical calculations give that, in the case of backward-bifurcating τ-periodic solutions, the amplitudes increase as the heating rate decreases. We find a homoclinic orbit at a particular value $\beta = \beta^{HO}$ at which the amplitude of the τ-periodic solution, branching off from the isolated convective solution, approaches the unstable steady solution with $x_1 \approx 0$. Simultaneously the period τ of the oscillatory solution tends to infinity as β^{HO} is approached from higher values of β. A stability

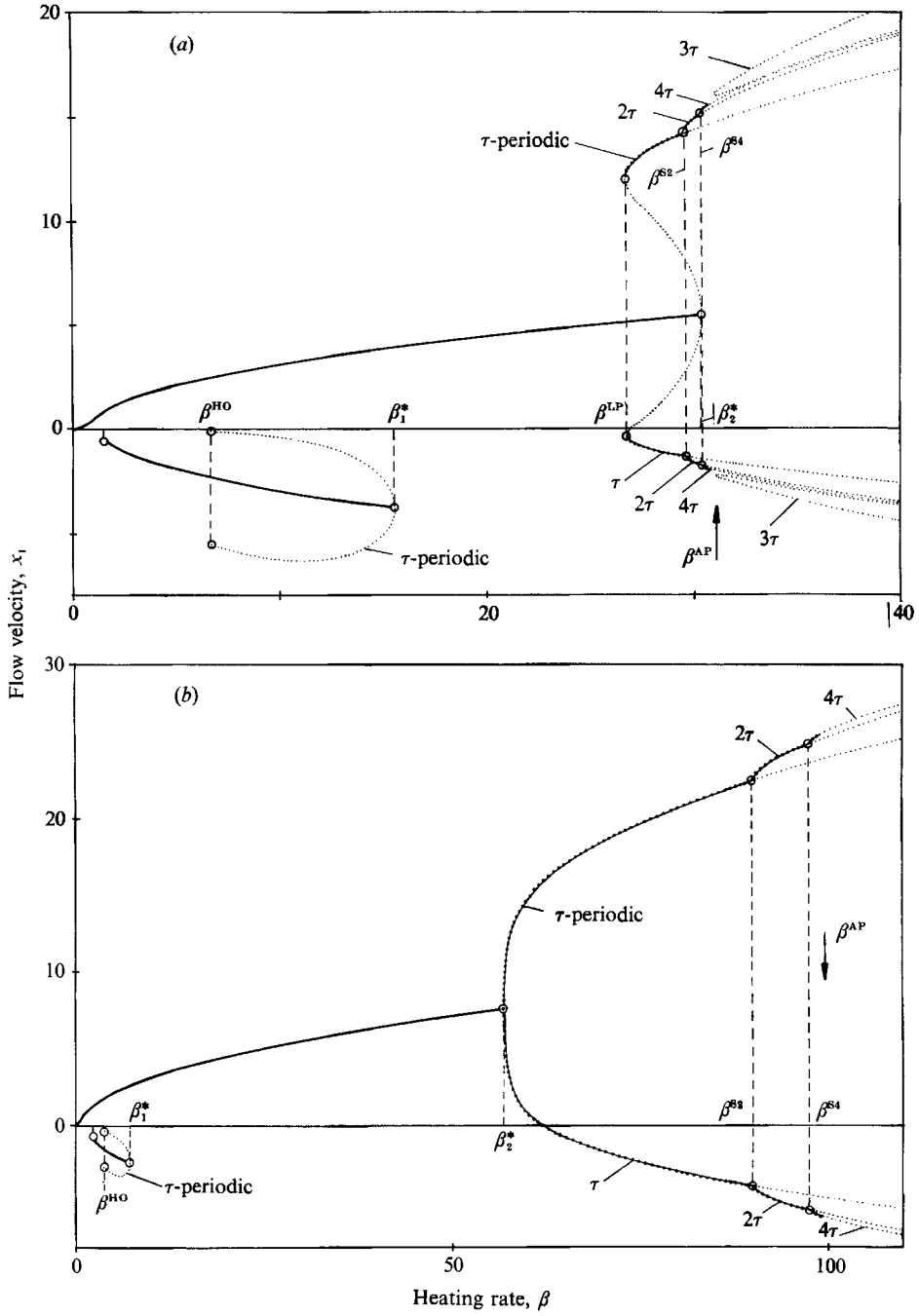

FIGURE 3. Bifurcation diagram for non-symmetric heating in terms of the velocity in the loop: (*a*) $\delta = 5°$, (*b*) $\delta = 15°$ ($\alpha = 15, K = 0$); solid lines represent stable steady branches, ○ mark stability bounds, dotted lines give amplitudes of periodic solutions, connected dots mark stable ranges of the periodic solutions. (Theoretical stability bounds: (*a*) $\beta_1^* = 15.6$, $\beta_2^* = 30.40$, $\beta^{HO} = 6.8$; (*b*) $\beta_1^* = 7.27$, $\beta_2^* = 56.91$, $\beta^{HO} = 4.06$.)

analysis shows, moreover, that the periodic solution in this range $\beta^{HO} \leqslant \beta < \beta_1^*$ is locally unstable while the steady solution is conditionally stable with respect to finite-amplitude disturbances.

For moderate values of the non-symmetry parameter δ the τ-periodic solution branching off backwards from the preferred steady convective solution develops a limit point at a value $\beta^{LP} = 26.8$, where the solution branch changes direction. This can be seen in figure 3(*a*). The stability analysis shows that the τ-periodic solution is unstable to infinitesimally small disturbances on the backward-directed part of its branch in the range $\beta^{LP} < \beta < \beta_2^*$, but stabilizes at the limit point. The stable character is maintained on the forward-directed part of the branch until, at a value β^{S2}, a subharmonic 2τ-periodic solution bifurcates from the τ-periodic solution. While the τ-periodic solution loses stability, the 2τ-periodic solution is stable until, at an even higher value β^{S4}, a 4τ-periodic solution branches off from the 2τ-periodic one. Increasing β more and more we find a set of $2^n\tau$-periodic solutions ($n \geqslant 1$), each member of which successively loses its stable character at the next bifurcation point, where another higher-order subharmonic solution occurs. In other words, we find that the subharmonic solution of highest possible order at a particular value of the heating rate β is stable. The above situation is commonly also referred to as a 'period-doubling sequence' (see e.g. Sparrow 1982).

The numerical calculations have been performed up to the 16τ-periodic solution and one result is that the interval length $\Delta\beta^{S2^{(n+1)}} = \beta^{S2^{(n+1)}} - \beta^{S2^n}$ between successive bifurcation points diminishes with increasing n. We therefore conjecture the existence of an accumulation point for the cascade of subharmonic bifurcations at a finite value of the control parameter β, denoted by the value β^{AP}. This accumulation point appears at some distance from the first subharmonic bifurcation point as the heating rate is increased. For heating rates $\beta > \beta^{AP}$ we expect an irregular, chaotic time behaviour of the system, since the system exhibits an infinite number of unstable periodic and steady solutions.

The above sequence of bifurcations, when the distance between bifurcations is rapidly decreasing, has been described generally by Feigenbaum (1980). He claims that the ratio of distances of successive bifurcations is governed by a geometric series of ratio f_∞. Thus within the bifurcation sequence the ratio

$$f_n = \frac{\Delta\beta^{S2^{(n+1)}}}{\Delta\beta^{S2^{(n+2)}}} \tag{11}$$

should rapidly converge for increasing n to the fixed value $f_\infty = 4.669\ldots$. We find from our sequence $f_1 = 4.48, f_2 = 4.62$. Thus, using the universal constant f_∞, we can evaluate the position of the accumulation point as $\beta^{AP} = 30.59$.

From our numerical investigations we infer that stable time-periodic solutions exist in the interval between the limit and the accumulation point, $\beta^{LP} < \beta < \beta^{AP}$. This stable 'window' is indicated in figure 3 by thin solid and (simultaneously) dotted lines, corresponding to stable periodic solutions. For clarity only the first three stable periodic solutions of the subharmonic cascade are shown, denoted by τ, 2τ and 4τ. Figure 3(*a*) also shows the calculated 3τ-periodic solution. This unstable solution is not connected to the $2^n\tau$-periodic solutions in the range of parameters investigated and exists for heating rates $\beta > \beta^{AP}$.

The situation of strong non-symmetry, characterized by $\delta = 15°$, is displayed in figure 3(*b*). The bifurcation of the τ-periodic solution at the Hopf point $\beta = \beta_2^*$ is forward-directed. Thus, there is no range with subcritical instabilities. Beyond the

stability limit β_2^* of the preferred steady flow a stable periodic solution exists in the range $\beta_2^* < \beta < \beta^{AP}$. The upper bound of this range is – as in the previously discussed case of $\delta = 5°$ – assumed to be given by an accumulation point β^{AP} of a cascade of subharmonic bifurcations. In this case, according to Feigenbaum, we find the ratios $f_1 = 4.28$ and $f_2 = 4.52$, and the position of the accumulation point is evaluated as $\beta^{AP} = 100.02$. The range $\beta > \beta^{AP}$ is absolutely unstable as in the case of moderate non-symmetry. In the sense of Gorman *et al.* (1986) this range can also be characterized as a range of globally attracting chaos. The numerical investigations indicate that there is a continuous transition from the backward- to the forward-directed bifurcation of the periodic solutions when δ is increased monotonically from zero.

In summary, for the case of a moderate non-symmetry in the system (see figure 3*a*), we find the following phenomena:

(i) For a continuous small variation in the control parameter β, a stable steady flow in one preferred direction always occurs. This flow is absolutely stable, i.e. with respect to disturbances of any size, in the range $\beta_1^* < \beta < \beta^{LP}$. For values $\beta \leqslant \beta_1^*$ large disturbance amplitudes may cause a transition to the isolated steady solution. In the range between the limit point and the Hopf point, i.e. for values $\beta^{LP} \leqslant \beta < \beta_2^*$, the preferred solution is conditionally stable, since finite-amplitude disturbances can drive the system into a stable or unstable $n\tau$-periodic oscillation depending on the parameters δ and β. For heating rates beyond the accumulation point at values $\beta > \beta^{AP}$ the system will fall into chaotic behaviour, in which the time-average values of the variables of state x_i are shifted towards the value of the respective unstable steady solution.

(ii) In order to establish a steady convective flow described by the isolated branch of the solutions, disturbances of large amplitude have to act on the system. This solution is only conditionally stable with respect to finite-amplitude disturbances, since a stable steady branch as well as the unstable τ-periodic orbit coexist. For large disturbances the system will therefore undergo a subcritical transition to the stable steady flow of opposite direction.

For the case of a strong non-symmetry in the system (see figure 3*b*), we find a forward-bifurcating stable τ-periodic solution at the Hopf point of the preferred steady solution. Therefore no subcritical instability will occur. This implies that the preferred steady solution is absolutely stable in the whole range $\beta_1^* < \beta < \beta_2^*$ and a locally stable periodic behaviour will occur for $\beta_2^* < \beta < \beta^{AP}$.

2.5. *Influence of fluid and wall properties*

The mechanical and thermal properties of the fluid and the tube walls enter the dimensionless model equations (8) in form of the parameters α and K. We emphasize that we have neglected the heat conduction in the flow direction. In a detailed analysis, Ehrhard (1988) has shown that heat conduction in the toroidal direction has an effect of negligible magnitude on the lower modes of the temperature series expansion (3). These modes determine the large-scale temperature variation along the loop and the flow velocity depends only on the lowest of those modes, i.e. on S_1 and C_1 (compare (7*a*)). He finds, however, a considerable effect on the higher modes, which describe the fine-scale structure of the temperature distribution in the loop.

We first discuss the influence of the fluid/wall parameter α, which can be considered as a modified Prandtl number. It can be seen from (8) that the steady-state solutions do not depend on the fluid/wall parameter α. There is, however, a

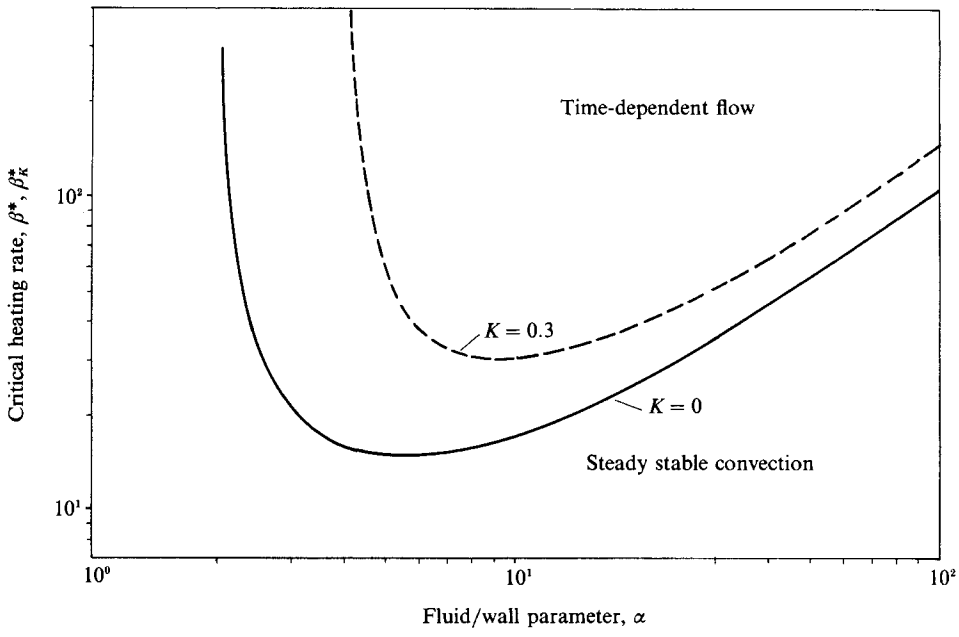

FIGURE 4. Stability diagram for the onset of time-dependent flow for symmetric heating ($\delta = 0°$); solid line refers to a constant heat transfer coefficient ($K = 0$) and dashed line to a velocity-dependent heat transfer ($K = 0.3$); both lines give states of neutral stability according to a linear stability analysis.

strong effect of α on the stability bounds β^*, β_1^* and β_2^* of the steady solution branches. This is demonstrated in figure 4 where the curves of neutral stability are given in the (α, β)-plane for the symmetric heating condition $\delta = 0°$.

We consider first in figure 4 the neutral stability curve for $K = 0$. This curve corresponds to the situation of a constant heat transfer coefficient, which is a basic feature of the Lorenz model (see Lorenz 1963). The graph displays the Hopf points β^* as a function of the parameter α. This curve is given by the analytical relation

$$\beta^*(\alpha) = \frac{(\alpha^2 + 4\alpha)}{(\alpha - 2)}. \tag{12}$$

All points below the curve represent states of stable steady convection, while for all points above the $\beta^*(\alpha)$ curve a time-dependent flow results.

A detailed study of the eigenvalues reveals purely real eigenvalues for $\alpha < 2$ and a pair of complex eigenvalues for $\alpha > 2$. Therefore the singularity of the function (12) at a value $\alpha = 2$ separates asymptotically stable behaviour for $\alpha < 2$ from oscillatory stable or unstable behaviour for $\alpha > 2$. Physically, small values of α correspond to an extremely good heat transfer at the fluid/wall interface. A stable flow for any parameter combination $\beta, \alpha < 2$ is therefore predicted for such conditions because any temperature disturbance is immediately suppressed. This prevents a feedback of such temperature disturbances after one cycle and leads to exponentially decreasing disturbance amplitudes.

These results concerning the Lorenz model agree with those reported by Robbins (1977) in a different physical context. Robbins also investigates numerically the dependence of the homoclinic bifurcation point on the fluid/wall parameter α. We discuss this aspect in §4.

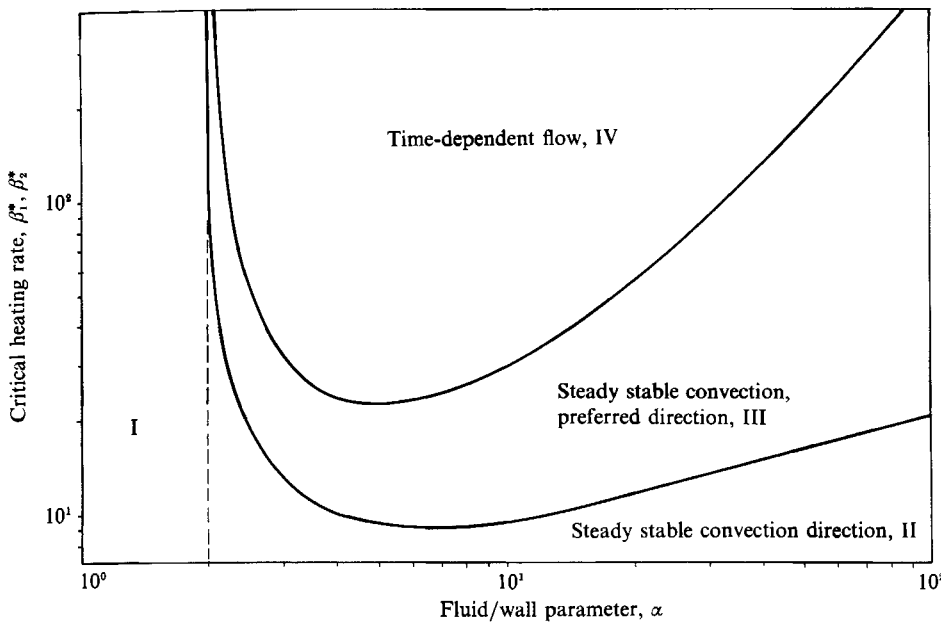

FIGURE 5. Stability diagram for the onset of time-dependent flow for non-symmetric heating, $\delta = 10°$ ($K = 0$); solid lines give states of neutral stability according to a linear stability analysis.

Next we consider the effect of the more realistic heat transfer law, equation (6). The parameter K only weakly affects the steady-state solutions, but has a strong influence on their stability bounds β_K^*. In figure 4 the result of a linear stability analysis is given for a value $K = 0.3$. We see from figure 4 that the critical heating rate for the onset of time-dependent flow is given by values $\beta_K^* > \beta^*$. This clearly indicates a stabilization of both steady solutions for $K = 0.3$ compared to the case $K = 0$. Moreover, the range of asymptotic stability is increased, as the singularity in $\beta_K^*(\alpha)$ moves to values $\alpha > 2$. Thus, an improved heat transfer at the fluid/wall boundary due to increased flow strongly stabilizes the steady convective flow.

A stability diagram of the steady solutions for a case of non-symmetric heating with $\delta = 10°$ is given in figure 5. The curves are given for a constant heat transfer coefficient h_W with $K = 0$. Since the stability bounds of the two steady convective solutions with opposite flow directions have different values β_1^* and β_2^*, two curves $\beta_i^*(\alpha)$ are presented in figure 5. The upper one represents states of neutral stability related to the preferred steady solution. The lower curve gives the states of neutral stability related to the isolated steady solution. Thus the (α, β)-plane in figure 5 is divided into four regions. In region I, characterized by $\alpha \lesssim 2$, the convective flow is asymptotically stable. In region II, stable steady convection can exist in either a clockwise or counterclockwise direction. Region III admits only the stable convection in the preferred counter-clockwise direction, determined by the non-symmetry parameter δ. No steady convection occurs for parameters α, β in region IV.

3. Experiments

3.1. *Experimental set-up*

The experimental set-up consists of a circular glass loop of radius $l = 31.3$ cm and tube diameter $d = 1.7$ cm. We use water as a test fluid yielding a fluid/wall

parameter of $\alpha \approx 15$. The parameter α is determined in the actual test apparatus by measuring the friction coefficient $f_W(u)$ as well as the heat transfer coefficient $h_W(u)$ for forced convection in a reasonable range of flow rates. From these measurements the heat transfer correlation gives $K \approx 0.35$ (see (6)). A detailed description of the preliminary measurements is given in §3.2.

The wall temperature of each quarter-circle of the tube is controlled separately, giving a temperature distribution along the tube walls which is a step function. This is achieved by circulating water through coaxial jackets at high volumetric flow rates, with a typical accuracy of about ± 0.05 °C in the controlled wall temperatures. Moreover, we have to account for a deviation from the ideal circular loop geometry because straight pieces of tubes of length $\Delta s = 13.0$ cm have been used as connecting parts between two semicircular glass tubes. These connections are arranged at $\varphi = 90°$ and $\varphi = 270°$. The experimental set-up is shown in figure 6, in which the position of the water jackets is given by the dotted areas. In three experiments, the non-symmetry angle of heating, δ, is adjusted to $\delta = 0°$, $\delta = 10°$ and $\delta = 15°$.

As can be inferred from §2.1, the leading-order Fourier coefficients of the wall temperature distribution Q_1 and R_1 determine the angle of symmetry δ. Thus the inclination of the heated and cooled sections within the gravitational field proves to be equivalent to the establishment of an odd wall temperature distribution ($Q_1 \neq 0$). In order to obtain a non-symmetric heating configuration, $\delta \neq 0$, we therefore adjust the wall temperatures within the separately controlled quarter circles accordingly rather than rotate the whole test apparatus.

The deviation of the experimental geometry, because of the form of the connecting parts, from the ideal case can be taken into account. For that reason we recall the treatment of the basic equations (1), which have been integrated once around the loop within Galerkin's method. If we account for the vertical straight pieces within the integration of the momentum equation we obtain

$$\left\{1+\frac{\Delta s}{\pi l}\right\}\frac{\mathrm{d}u}{\mathrm{d}t} = \frac{\gamma g}{2\pi}\left\{\int_0^{2\pi} T(\varphi)\sin(\varphi)\,\mathrm{d}\varphi + \int_0^{\Delta s/l} T(\tfrac{1}{2}\pi)\,\mathrm{d}s - \int_0^{\Delta s/l} T(\tfrac{3}{2}\pi)\,\mathrm{d}s\right\} - \left\{1+\frac{\Delta s}{\pi l}\right\}\tfrac{1}{2}u f_{W0}. \quad (13)$$

It is justifiable to consider those sections as thermally insulated, since, except for a hole of 2 mm in diameter for velocity measurements, these tubes are surrounded by insulating material during the experiment. For that reason the heat transport equation remains unchanged, while we have constant average temperatures along these adiabatic vertical segments. We introduce an adapted scaling for the temperature coefficients S_1 and C_1 as

$$\left.\begin{aligned} x_2 &= \frac{\rho_0 c_p}{h_{W0}}\frac{\gamma g}{f_{W0} l}\frac{\left(1+2\dfrac{\Delta s}{\pi l}\right)}{\left(1+\dfrac{\Delta s}{\pi l}\right)} S_1, \\ x_3 &= \frac{\rho_0 c_p}{h_{W0}}\frac{\gamma g}{f_{W0} l}\frac{\left(1+2\dfrac{\Delta s}{\pi l}\right)}{\left(1+\dfrac{\Delta s}{\pi l}\right)}\left\{\frac{\rho_0 c_p}{h_{W0}} R_1 - C_1\right\}, \end{aligned}\right\} \quad (14)$$

while the other quantities remain scaled according to (5). Using a procedure

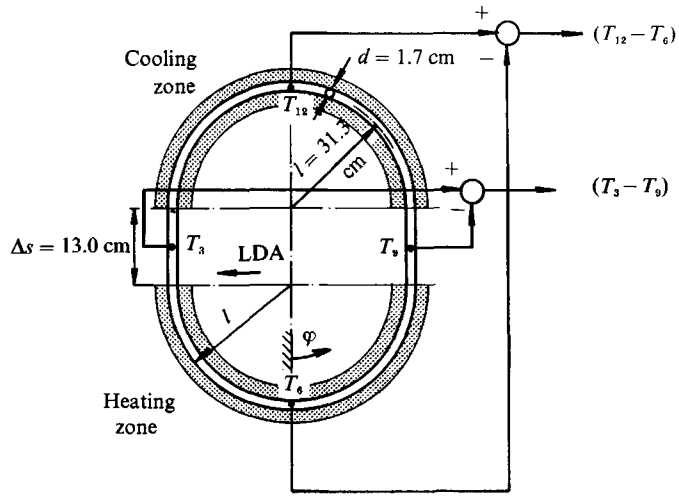

FIGURE 6. Sketch of the experimental set-up.

analogous to that in §2.1 we obtain the approximate set of ordinary differential equations

$$\left.\begin{aligned} \dot{x}_1 &= \alpha[x_2 - x_1], \\ \dot{x}_2 &= \beta_e x_1 - x_2[1 + K|x_1|^{\frac{1}{3}}] - x_1 x_3 + \beta_e \tan\delta, \\ \dot{x}_3 &= x_1 x_2 - x_3[1 + K|x_1|^{\frac{1}{3}}]. \end{aligned}\right\} \tag{15}$$

Herein an effective heating β_e occurs as modified parameter, which is defined by

$$\beta_e = \frac{1 + 2\dfrac{\Delta s}{\pi l}}{1 + \dfrac{\Delta s}{\pi l}} \beta. \tag{16}$$

We therefore conclude that by using the appropriate scaling and parameters the experimental set-up is a physical representation of the employed model equations (8).

The measuring equipment includes a laser Doppler anemometer (LDA) for monitoring the flow velocity $u \propto x_1$, and thermocouples of 0.1 mm in diameter for measuring the horizontal and vertical temperature differences inside the loop, $(T_3 - T_9)$ and $(T_{12} - T_6)$. We employ a helium neon laser (632.8 nm), two Bragg cells operated with a shift of 25 kHz and a photomultiplier positioned in the forward-scatter direction within the optical part of the LDA. Burst analysis is performed by means of a transient recorder in conjunction with a Z89 microcomputer on the basis of 'zero crossing detection'. Thermocouple voltages are amplified differentially using high-performance differential amplifiers. The typical resolution achieved is ± 0.02 cm/s for the velocity and ± 0.05 °C for the temperature differences. With the aid of these temperature differences the basic modes of the temperature distribution, x_2, x_3, can be evaluated. All experimental data are taken in the centre of the cross-section A of the pipe. Based on preliminary measurements of velocity and temperature profiles along the diameter of the tube we are then able to estimate the average value of a quantity on the basis of the local centre value (compare §3.2). The overall configuration of local velocity and temperature measurements prove to resolve frequencies of up to 2 Hz for the case of the LDA and frequencies up to 30 Hz

for the case of thermocouples. Both cut-off frequencies are considerably higher than any observed frequency in the experiment. In addition to the local measuring techniques outlined above, we occasionally used tracer material and a laser-light-sheet method to visualize three-dimensional flow structures in certain sections of the loop.

In order to allow a comparison of our experimental procedure with other procedures, i.e. of Creveling *et al.* (1975), Damerell & Schoenhals (1979), Gorman *et al.* (1986), we give some typical experimental ranges of the physical quantities. The temperature differences ΔT between heated and cooled wall regions lay in the range $0 \leqslant \Delta T \leqslant 52$ °C, while the heat flux q_W established per unit wall area varied within the interval $0 \leqslant q_W \leqslant 0.56$ W/cm^2. The variables of state were measured within the ranges $-4.5 \leqslant u \leqslant 4.5$ cm/s, $-12 \leqslant (T_3 - T_9) \leqslant 12$ °C and finally $-5 \leqslant (T_{12} - T_6) \leqslant 2$ °C. Under time-dependent conditions the main frequency of oscillation f is usually very close to the frequency given by a particle travelling with the mean velocity u around the loop. The measured data on the basis of power density spectra lay in the interval $3 \leqslant f \leqslant 19$ mHz.

All of the experimentalists cited above applied a constant heat flux on the bottom half-circle of the loop, while the top half-circle was maintained at a constant temperature. The diameters of the flow channels used by them were 3.0 cm and 2.1 cm, respectively. We have, in contrast, used a smaller tube diameter of 1.7 cm in order to decrease the thermal diffusion time across the flow channel. Gorman *et al.* report a fluid/wall parameter in the range $3.1 \leqslant \alpha \leqslant 4.9$ in their experiments.

3.2. *Preliminary studies, experimental procedure*

In §2.1 we introduced correlations for the friction term f_W and the heat transfer coefficient h_W into the model. These correlations are both based on a forced flow within a circular straight tube. Therefore they are strictly valid only for equivalent conditions. In order to obtain correlations valid in the actual test apparatus we open the loop at a position $\varphi = 90°$ and provide a flow with adjustable mean velocity entering the test section smoothly through a straight tube of 1 m length and the same inner diameter. The fluid circulates around the loop and leaves the test section via a straight piece of tube. The average flow velocity is measured precisely by weighing the emerging fluid during fixed time intervals using a high-resolution electronic scale. The entrance fluid temperature is thermostated and the thermally non-active parts of the tubes are insulated. We use the same overall average fluid temperature in both the preliminary and the ordinary measurements, i.e. 30 °C. The differences of average temperature and of pressure between inlet and outlet are monitored by platinum resistance thermometers and a capacitive pressure transducer, both operated differentially.

The results from those measurements are given in figure 7, showing the pressure loss ($\propto f_W$) and the heat transfer coefficient ($\propto h_W$) both as function of the flow rate ($\propto u$). We have also included in the diagrams the correlations obtained from regressing the experimental data to a form as introduced by (2) and (6). Thus the constants from those model equations, namely f_{W0}, h_{W0} and K, are determined. Both dependencies prove to describe reasonably well the behaviour of the experimental data. Although we have accounted for the curved geometry of the tubes as present in the test apparatus, we point out that those correlations do not include any effects from three-dimensional flow patterns, probably caused by the natural convection. Very little quantitative information on such effects is available, however.

During our experiments we intend to perform steady and time-dependent

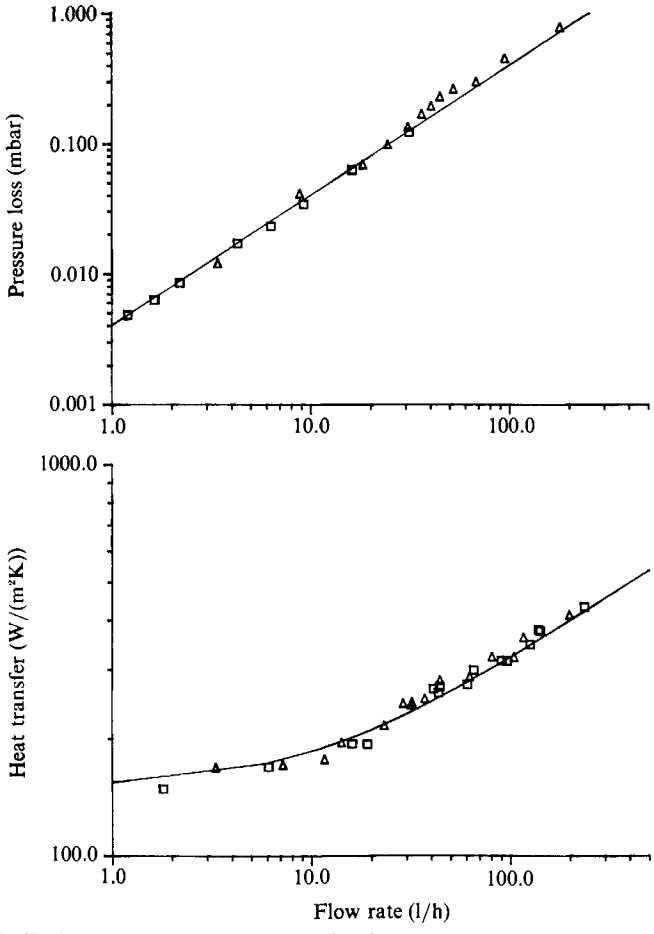

FIGURE 7. Preliminary measurements on the friction and heat transfer law in the actual test apparatus. △ and ◇ respectively give measurements using a positively or negatively oriented flow, solid lines give regressed model correlations.

measurements on the cross-sectionally averaged flow velocity and temperatures at certain positions. In order to obtain continuous and sufficiently time-resolved information we employ local measurements in the centre of the cross-section A, rather than scanning the cross-section at every time step. For that reason we have to provide a method allowing an estimation of the average value of a quantity if the value in the centre of A is given. The assumption of parabolic profiles across A obviously does not hold, since the curvature of the tubes establishes significantly different profiles in both temperature and velocity at certain positions.

For a set of 16 typical heating rates β we therefore perform *a priori* velocity and temperature measurements along the diameter of the tube at every probe position, and for both directions of the mean flow. From these data we are able to obtain correlations between the local centre value and average value of a quantity as function of the heating rate β. We use regression polynomials to generate analytical expressions for those correlations and to extrapolate them slightly towards lower and higher values of the heating rate β. Using these polynomials later in the ordinary measurements we can estimate the average value of a quantity on the basis of a measurement of the local centre value in a most accurate manner.

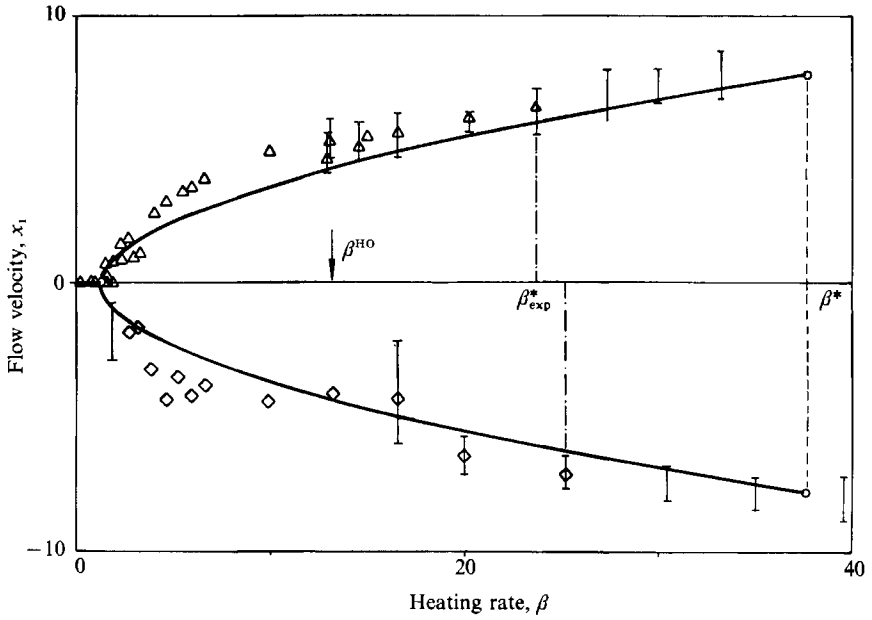

FIGURE 8. Measured velocities for symmetric heating ($\delta = 0°$); △ and ◇ give steady states, vertical bars mark maximum amplitudes of time-dependent flow, solid lines represent theoretical results for steady solutions and ○ mark their stability bounds (theoretical parameters $\alpha = 15, \delta = 0, K = 0.35$).

Finally we give a description of our method employed to find various bounds of stability. We use an extremely careful step-up procedure on the heating rate β (temperature difference ΔT) for typically at least three times in order to detect the highest value of the heating rate for which a steady stable flow is observed. Thus this method should provide an experimental equivalent β^*_{exp} to the theoretically obtained value β^*. The lower limit of a subcritical range, namely β^{HO} or β^{LP}, is experimentally approached in three different ways. First, a change of the heating rate β in major steps proves to introduce large perturbations. Secondly, a complete blocking of the flow for typically 10 to 15 minutes is used in order to generate large perturbations. This is achieved by means of a metal sheet inserted between the two semicircles just in the vertical connecting parts. Finally, a step-down procedure starting from an oscillating flow in the supercritical range is always employed until a transition to a steady stable flow is observed. We take the lowest value of the heating rate β where time-dependent flow is observed to be the lower bound of the subcritical region. Mostly this value results from the first method, i.e. from a variation of β in major steps.

Gorman *et al.* (1986) have used, in addition, an indirect experimental method to obtain information on the structure of the strange invariant set. In particular they use the time intervals between flow reversals as an indicator to determine whether or not the system tends to fall into a stable steady operation. Our experimental results do not allow for such a distinction.

3.3. *Experimental results for symmetric heating*

For a direct comparison between the model predictions and the experimental observations the dimensionless measured flow velocity, $x_1 \propto u$, is given as a function

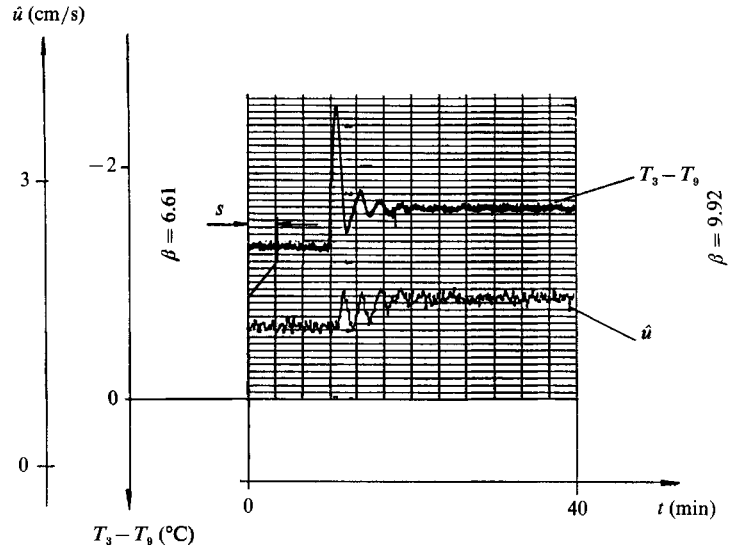

FIGURE 9. Example of a time history recorded in the stable steady range; curves correspond to $\hat{u} \propto x_1$ and $(T_3 - T_9) \propto x_2$, s indicates the offset of recorder.

of the measured heating rate $\beta \propto \Delta T$. Thus, figure 8 corresponds completely to the theoretical results for symmetric heating, given in figure 2. The experimentally observed steady states and the predicted steady states, including stability bounds, are given in figure 8.

In agreement with the theory, we find, in a small region $0 \leqslant \beta \leqslant \beta^0_{\text{exp}}$, a state of rest without any circulating flow in the loop. This state obviously admits only diffusive heat transport from the high- to the low-temperature region in the loop. An increase of the heating rate β above a first critical value β^0_{exp}, results in a steady convection flow in either a clockwise or counter-clockwise direction, depending on the initial perturbation. When the experiment is carefully conducted by increasing β in sufficiently small steps, a steady flow persists up to a heating rate β^*_{exp} indicated by dashed-dotted lines in figure 8. For values $\beta > \beta^*_{\text{exp}}$ a time-dependent fluctuating flow is observed for any size of disturbance affecting the flow. The maximum variation of the velocity x_1 of such time-dependent convection is marked in figure 8 by vertical bars.

Thus we find reasonable agreement between the predicted flow rate x_1 and the measured data for the steady convection in both flow directions. There is a discrepancy between the predicted and the observed bounds of linear stability for the steady flow; we have $\beta^* > \beta^*_{\text{exp}}$. We conjecture that this discrepancy is on one side due to the differences between the assumptions made in a linear stability analysis and the real experiment where perturbations of finite amplitude are usually present. We find also a difference in the two values β^*_{exp} for the flow in a clockwise and counterclockwise direction, which indicates a small, but unidentified, asymmetry in the experimental set-up. On the other hand, the theoretical stability bound β^* depends strongly on K, the parameter in the heat transfer law. Therefore an inaccuracy in the experimentally determined value could also explain the present discrepancy.

Next we outline some typical nonlinear features of our experimental observations. We discuss three typical experimentally recorded time histories of the temperature

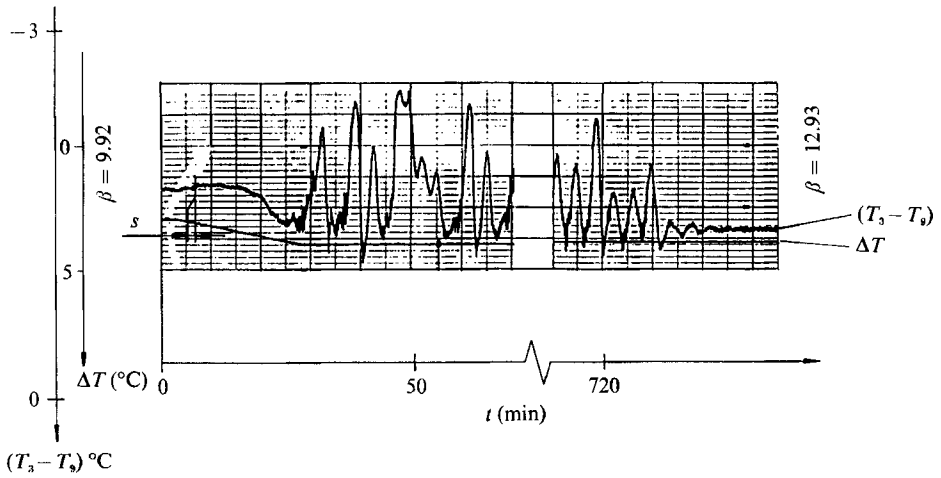

FIGURE 10. Example of a time history in the subcritical range; curves correspond to $\Delta T \propto \beta$ and $(T_3 - T_9) \propto x_2$, s indicates the offset of recorder.

and the velocity, and compare theoretical predictions. Figure 9 illustrates a transition from one steady state of convection to another steady state at an elevated level of the temperature difference $\Delta T \propto \beta$. This transition is initiated by a sudden stepwise increase of the driving temperature difference ΔT. It can be seen that, a few minutes after the significant change in β at time $t = 0$, the state variables $\hat{u} \propto x_1$ and $(T_3 - T_9) \propto x_2$ adjust, via a stable oscillatory transient, to new stationary conditions. We have established in repeated tests that, independent of the size of the applied temperature increment, only stable steady flow results in a range of moderate values of β. In figure 8 the measured states in this flow regime are denoted by the symbols $\triangle$ and $\diamond$ without a vertical bar.

A typical temporal behaviour of the system in the subcritical region is shown in figure 10. After a major ramp-type increase of the heating rate $\beta \propto \Delta T$ starting at $t = 0$, we observe an oscillatory temporal behaviour of the measured temperature difference $(T_3 - T_9) \propto x_2$ for an extended period of about 700 min. Then without changing the external parameters of the system a spontaneous relapse into the steady state occurs. We can also realize the identical steady state if we increase β in several sufficiently small steps. By such a procedure the oscillatory temporal behaviour is avoided and the final steady state is established via a sequence of stable oscillatory transients. Figure 10 thus illustrates the two observed states that may occur in the subcritical range for small and for finite-amplitude perturbations at identical values of the heating rate β. The subcritical region realized in the experiments is in fact characterized by the possible occurrence of a steady or alternatively an oscillatory flow. In figure 8 this dual state is indicated by the combined symbols for steady and time-dependent flow. The experiments also demonstrate the potential transition of the system from an oscillatory state to a steady state in the long term. This particular phenomenon, however, does not necessarily occur in finite measurement intervals and is rarely observed during the experiments.

In figure 11 we present, as a typical sample of our history records, the temperature difference $(T_3 - T_9) \propto x_2$ in the absolutely unstable range $\beta > \beta^*_{\text{exp}}$. In agreement with our theoretical conclusions we observe a chaotic time behaviour independent of the sampling interval. The changes in the sign of the temperature difference $(T_3 - T_9)$ at

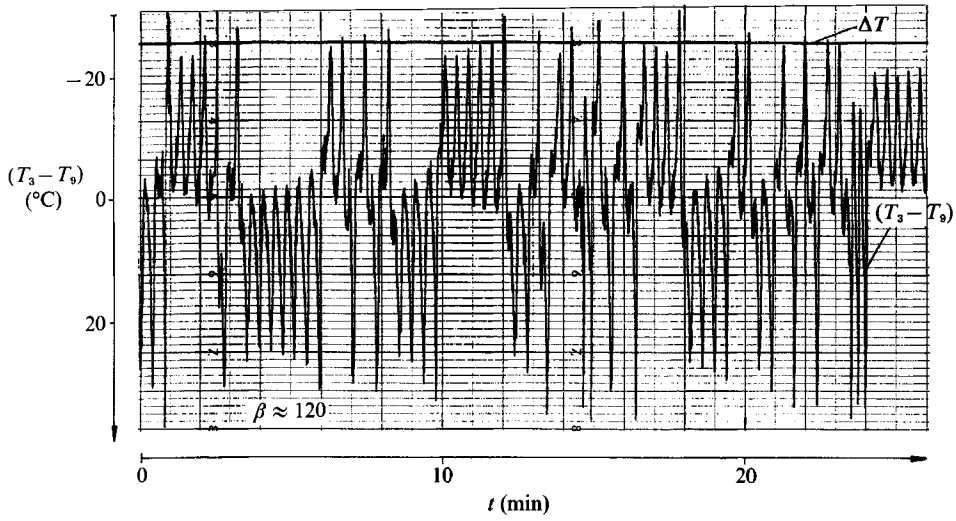

FIGURE 11. Example of a time history in the absolutely unstable range; curves correspond to $\Delta T \propto \beta$ and $(T_3-T_9) \propto x_2$.

certain times are linked to reversals of the flow direction in the loop occurring at random increments of time. This can be explained with the aid of figure 6. The temperature difference (T_3-T_9) is measured between the vertical sections of the loop. Since a flow, e.g. in the counter-clockwise direction, will transport hot fluid to the T_9 while cold fluid passes the T_3 position we observe $(T_3-T_9) < 0$. Accordingly, for flow in a clockwise direction we find $(T_3-T_9) > 0$.

We note here explicitly that we observed self-induced flow reversals only for very high heating rates of $\beta \gtrsim 120$. In the range of $\beta^*_{\text{exp}} < \beta < 120$ a flow with chaotic time behaviour and flow reversals could only be generated by major external excitations, e.g. large sudden jumps in the heating rate. Without external perturbations we find oscillatory flow with random character and bounded amplitudes in either a clockwise or counterclockwise direction. The time behaviour of the flow therefore does not indicate any flow reversals and it resembles the behaviour obtained during oscillatory portions within the subcritical range (compare figure 10).

It is important to notice that in both cases where limited-amplitude oscillations are observed, i.e. in the subcritical region and the moderate-supercritical region, an explanation of the dynamics purely on the basis of the Lorenz model is not possible. We find, however, that the power density spectra of the signals observed in those regions are similar to those spectra expected from the Lorenz model as far as the lower frequency range, associated with the mean motion, is concerned (see Ehrhard 1988). However, those spectra, in addition, contain large portions of power within considerably higher frequencies, which cannot be explained by the one-dimensional model.

We attribute the delayed occurrence of the oscillatory convection with flow reversals in both the subcritical and the moderate supercritical range to local two- and three-dimensional flow perturbations, which change the overall friction losses and reduce buoyancy by levelling out temperature gradients. In fact using a laser-light-sheet method and tracers we have identified zones of recirculating flow at the inboard side of the vertical sections of the loop (see Ehrhard 1988). These recirculation zones are observed in all states of convection. However, they affect the

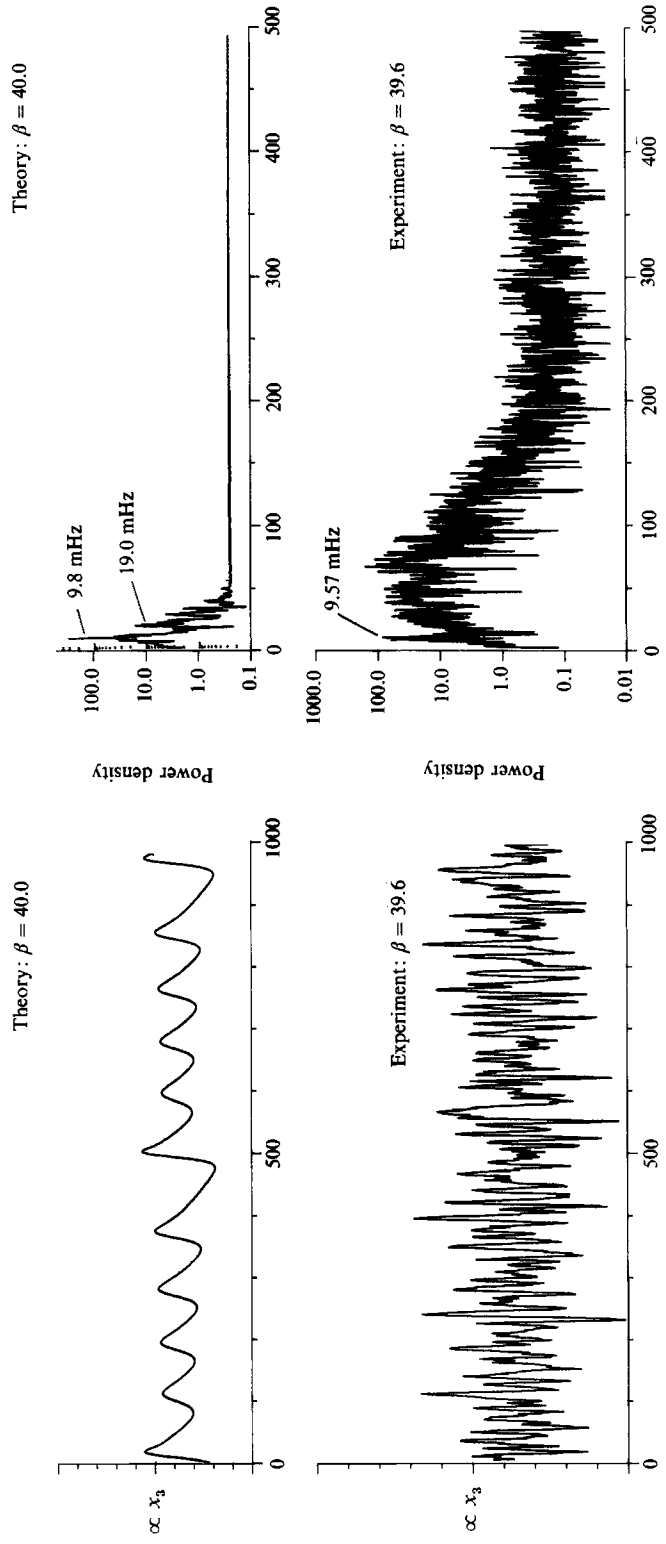

FIGURE 12. Comparison between experimentally and theoretically obtained power density spectra in the moderate-supercritical range (theoretical parameters: $\alpha = 15, \delta = 0, K = 0.35$).

otherwise mainly one-dimensional flow severely only when large-amplitude oscillations occur. The above arguments are supported quantitatively by comparing the power density spectra which are obtained from a direct numerical integration of the model equations (8) with the experimentally recorded temperature histories. In figure 12 we give a typical set of signals x_3 and related spectra, obtained in the moderate-supercritical range. In both the theoretical and the experimental cases we first compute the autocorrelation function in the time domain and from this we obtain the power density spectra via a Fourier transformation. A fourth-order Runge–Kutta scheme is used for the direct numerical integration of (8). We confirm from figure 12 corresponding peaks in the experimental and theoretical spectra at 9.8 mHz and 9.57 mHz. A major portion of power in the range 30–120 mHz, however, is present in the experimental spectrum, which presumably is due to locally three-dimensional flow pattern. Ehrhard (1988) shows, moreover, that in addition to the contribution of the mean-flow oscillations at relatively low frequencies, an increased contribution of higher-frequency oscillations to the power density spectra is obtained by measuring inside those recirculation zones in the absolutely unstable range.

Our observations have some features in common with the experimental findings of Creveling *et al.* (1975) and Gorman *et al.* (1986). These authors performed similar experiments in a symmetrically heated circular loop with a constant wall heat flux in the lower and constant wall temperature in the upper semicircle of the loop. At moderate heating rates, two steady convective flows, one clockwise, the other counter-clockwise, are observed by all investigators. At high heating rates, they all find oscillatory flow of chaotic character exhibiting global flow reversals at times. Creveling *et al.* report that they realize an intermediate stable unsteady state with periodic temperature oscillations. It may be conjectured that this oscillatory state observed by Creveling *et al.* corresponds to the subcritical oscillatory states which Gorman *et al.* and ourselves find, if finite-amplitude disturbances act on the convection. Gorman *et al.* attempt to explain the 'stable oscillations' of Creveling *et al.* by a 'crisis' theory of Greborgi, Ott & Yorke (1982) but admit that they were unable to measure any characteristics of this particular theory. They also suggest that in the subcritical range of heating rates, the oscillatory states should be subdivided into states of 'transient chaos' and 'subcritical chaos' depending on whether, after some residence time in the chaotic state, the system returns to the steady state or not. These authors use statistical means to support their idea. We have not particularly investigated the dynamical characteristics of the chaotic flow regime for $\beta \gtrsim 120$, because the high heating rates for achieving permanent chaotic states could not be sustained for extended experimental times without risking damage to the set-up. Finally, the flow in our experiments stays, contrary to the observations of Creveling *et al.*, laminar, but partly time-dependent, in the whole parameter range $0 < \beta \lesssim 200$. This is also clearly confirmed by the measured friction law $f_W(u)$, which retains a strictly linear dependency up to the highest measured flow velocities. This difference is obviously due to the different diameter of the tube used by Creveling *et al.*

3.4. *Experimental results for non-symmetric heating*

Experiments have been conducted for two different non-symmetry parameters δ, namely $\delta = 10°$ and $\delta = 15°$. The results of the first experiment using a non-symmetric heating configuration with $\delta = 10°$ are shown in figure 13. The experimental data corresponding to the continuous branch of the steady solutions

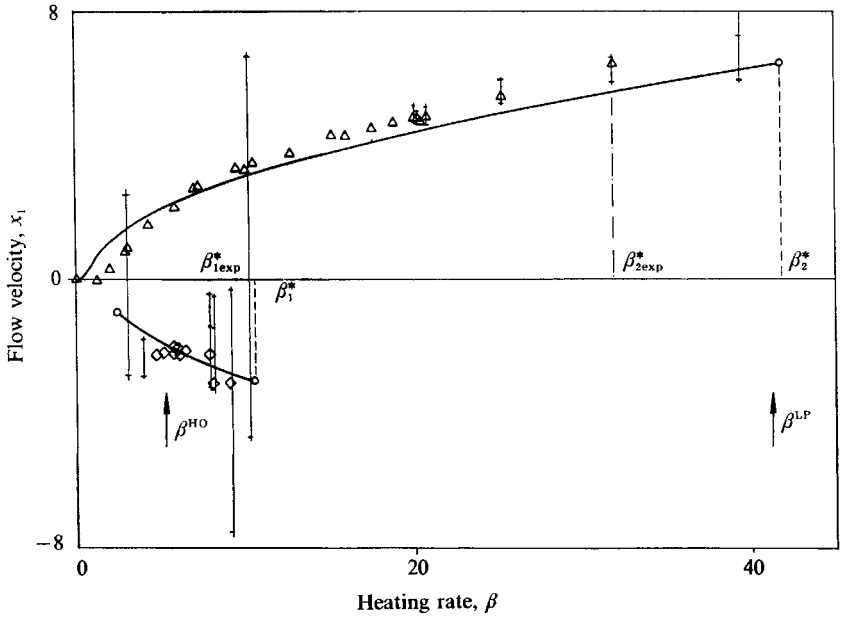

FIGURE 13. Measured velocities for non-symmetric heating ($\delta = 10°$); △ and ◇ give steady states, vertical bars mark maximum amplitudes of time-dependent flow, solid lines represent theoretical results for steady solutions and ○ mark their stability bounds (theoretical parameters: $\alpha = 15$, $\delta = 10°, K = 0$). (Theoretical stability bounds: $\beta^*_1 = 10.8, \beta^*_2 = 41.8, \beta^{HO} = 5.2, \beta^{LP} = 41.4$.)

are obtained by a gradual increase of the driving temperature difference $\Delta T \propto \beta$. We find steady flow in the preferred direction in a range $0 \leqslant \beta \leqslant \beta^*_{2\exp}$ if a sufficiently smooth step-up procedure is used in the experiment. The isolated steady-state flow is established by initially introducing specific perturbations into the wall-temperature distribution. Once a state of steady convection of this isolated branch is obtained, other neighbouring steady states are generated by slowly increasing or decreasing the driving temperature difference $\Delta T \propto \beta$. This is performed until the bounds of stability of this isolated steady-state flow are identified.

The experimental data for both states of convection are given in figure 13, and it can be seen that both data sets follow closely the two branches of the steady solutions predicted by the model. The experimental data on the steady flow with preferred flow direction indicate at low values of the heating rate velocities close to zero, although the temperature measurements $(T_{12} - T_6)$ and $(T_3 - T_9)$ clearly confirm the presence of a positively directed flow. We attribute this discrepancy to the method of evaluating the average velocity employed. Particularly at very small mean velocities, superimposed three-dimensional patterns may cause a considerably reduced value of the local velocity in the tube centre, which is used as the basis of this evaluation.

For values of $\beta > \beta^*_{2\exp}$ we find only time-dependent oscillatory flow. The maximum and minimum amplitudes occurring in this time-dependent regime are indicated by vertical bars in figure 13. The temperature records from our experiments do not indicate any global flow reversal in certain time intervals for $\beta > \beta^*_{2\exp}$. The theoretical results of figure 3 admit such reversals in principle. We attribute this discrepancy in our case once more to the increased dissipative effects of the local three-dimensional flow disturbances occurring – according to our observations – with higher intensity at higher values of the heating rate. In their experiments, Damerell

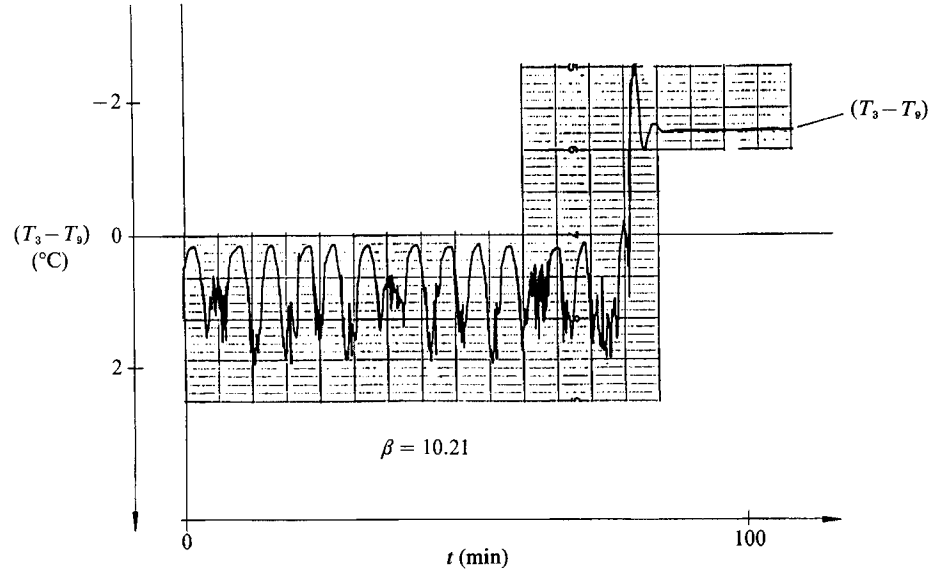

FIGURE 14. Example of a recorded transition from the subcritically unstable isolated steady state with clockwise flow direction to the preferred counterclockwise flow ($\delta = 10°$); the curve corresponds to $(T_3-T_9) \propto x_2$.

& Schoenhals (1979) have observed a limitation in the occurrence of oscillatory flow reversals for non-symmetry parameters $|\delta| < 6°$. They also report observations of two- and three-dimensional flow effects, to which they attribute indirectly the limitations of the flow oscillations. In particular they find that the evaluated volumetric flux in the loop is reduced by these effects. The basic features of such three-dimensional effects in a toroidal convection loop have recently been analysed numerically by Lavine, Greif & Humphrey (1987). The results of these authors qualitatively confirm the experimental observations.

We can also generate time-dependent oscillatory flow in a subcritical range of heating rates $\beta \leqslant \beta^*_{2\,\mathrm{exp}}$ if we introduce a perturbation of a large enough amplitude into the system. Usually, this is achieved by varying β in large steps. The extension of the observed subcritical region is recognized in figure 13 by the symbols for both steady and oscillatory convection.

The experiment confirms furthermore that the isolated branch of the steady solutions is bounded on both sides. We observe a transition of the clockwise-directed convection to a counter-clockwise flow when β reaches a lower and upper bound on the isolated branch. In figure 13 the experimental transitions are represented by two vertical bars which connect both branches of steady states. As a typical example figure 14 illustrates the transition process at the upper stability bound at a value $\beta = \beta^*_{1\,\mathrm{exp}}$ by a temperature history record. The record of the temperature difference (T_3-T_9) shows the manner in which the subcritically unstable, oscillatory, clockwise flow changes into a stable, steady flow with counter-clockwise orientation. This process is thus associated with one single flow reversal, since the sign of the temperature difference (T_3-T_9) depends strictly on the flow direction.

We conclude that the experiment with $\delta = 10°$ exhibits most of the essential features of the model. In particular, we find an imperfect bifurcation of the steady solutions including an isolated steady state as well as a preferred state of convection.

The experimental validation of existing subcritical instabilities strongly supports the existence of two backward-bifurcating, unstable periodic solutions, as predicted by the model equations (8). Moreover, there is a reasonable quantitative agreement between theory and experiment for the stability bounds β_1^* and β_2^*.

The second experiment is performed with a larger non-symmetry parameter, i.e. $\delta = 15°$, in order to verify the theoretical prediction of a forward-directed bifurcation of the τ-periodic solution at the Hopf point β_2^* of the preferred branch. For this particular situation a stable, time-periodic flow should arise in the loop for heating rates $\beta > \beta_2^*$.

The experiment with a non-symmetry angle of $\delta = 15°$ confirms mostly the predictions of the model for larger parameter values δ. The convective flow in the preferred positive φ-direction is clearly stabilized when compared to the first experiment with a moderate non-symmetry of $\delta = 10°$. The heating rate for the onset of oscillatory flow is clearly shifted to a value $\beta^*_{2\,\mathrm{exp},\,15°} > \beta^*_{2\,\mathrm{exp},\,10°}$. The experiments give $\beta^*_{2\,\mathrm{exp},\,15°} = 64.2$ and $\beta^*_{2\,\mathrm{exp},\,10°} = 31.7$. This implies that the stable range of the isolated branch is reduced and the transition to the preferred state of flow occurs at a heating rate $\beta^*_{1\,\mathrm{exp},\,15°} < \beta^*_{1\,\mathrm{exp},\,10°}$; here $\beta^*_{1\,\mathrm{exp},\,15°} = 7.0$ and $\beta^*_{1\,\mathrm{exp},\,10°} = 10.2$. The displacements of the stability bounds β_1^* and β_2^*, as well as the general character of the steady solutions, are in reasonable agreement with the theoretical findings.

However, contrary to the predictions of the model, we cannot realize experimentally a stable time-periodic flow. Instead we find a small range of heating rates β, where the steady states exhibit subcritically unstable features if sufficiently large perturbations are imposed to the flow. We also find that the extension of this subcritical region is smaller by a factor of 0.16 compared to the subcritical interval in the case of moderate non-symmetry (see figure 13). Thus the experiments support qualitatively the theoretical result that increasing non-symmetry will reduce the extent of the subcritical range and eventually turn the backward bifurcation into a forward one. We observe an oscillatory flow for $\beta > \beta^*_{2\,\mathrm{exp}}$, which clearly is not of periodic character. The observed oscillations of the temperature history agree qualitatively with those illustrated in figure 11. In summary, we again observe in this experiment most of the features related to a backward bifurcation of the unstable periodic solution from the steady state. During the measurements at higher heating rates β, i.e. for values $\beta \gtrsim 80$, however, we observe a considerable deviation of the actual wall-temperature distribution from the intended step function. Specifically the thermocouples in the coaxial water jackets monitor a major difference between inlet and outlet temperatures, which are due to the amount of heat transferred. Since this deviation reduces the effective non-symmetry parameter δ, a careful evaluation of the observations, especially in the supercritical range, does not provide a clear judgement of whether a backward or forward bifurcation from the stability bound of the steady flow, i.e. at $\beta = \beta^*_{2\,\mathrm{exp},\,15°}$, is present.

4. Discussion

As a detailed comparison between the calculated results from the analytical model and the experimental findings, we summarize those particular features of the model which are in principle observable in an experiment. We discuss them in the order of increasing heating rates starting with the symmetrically heated loop. We also compare our results with the results of other authors, if available.

(*a*) The model equations predict a stable state of rest (we term it a 'heat conduction solution') in the range $0 \leqslant \beta < \beta^0$ for the symmetrically heated loop. This

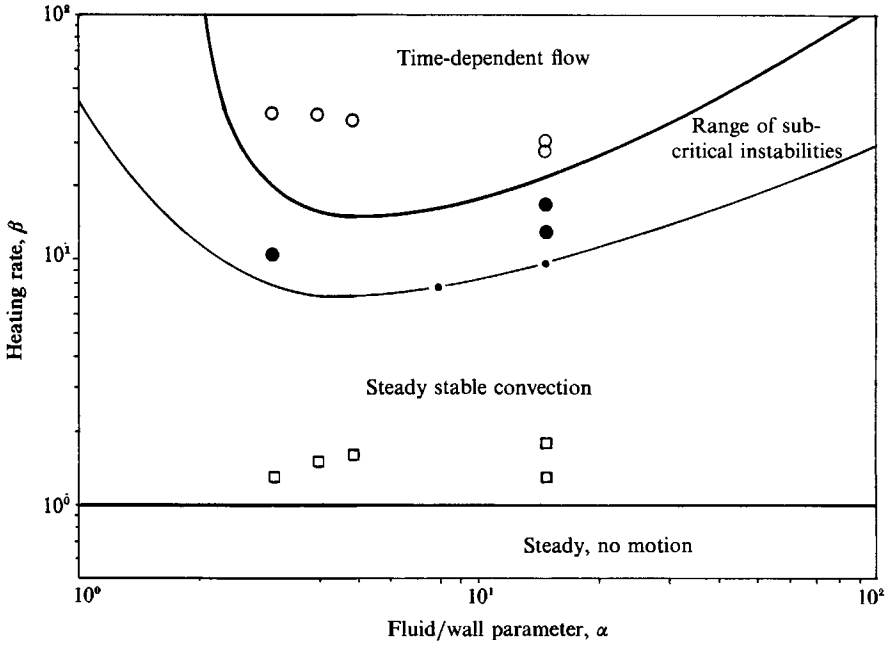

FIGURE 15. Stability diagram for symmetric heating conditions. Theory: thick solid lines refer to stability bounds according to a linear perturbation analysis, thin solid line represents nonlinear calculations of Robbins (1977) for the heating rate at the homoclinic orbit, · indicates present results at the homoclinic orbit (parameters: $\delta = 0, K = 0$). Experiment: □ indicate onset of convection, ● mark the first occurrence of subcritical instabilities, ○ indicate the limit of the absolutely unstable range.

behaviour of the system is confirmed by the experiments, since there is a range of heating rates where no convection is observed in the loop. The observed onset of convection reported by Gorman *et al.* (1986) for different values of the fluid/wall parameter α in the range $3 < \alpha < 5$ and also our measurements for $\alpha = 15$ indicate that there is no significant dependency of the critical heating rate for the onset of convection on the parameter α. In figure 15 these data are indicated by symbols □ in a stability diagram plotted in the (α, β)-plane. The observations are therefore compatible with the theoretical results predicting the onset of convection at a value $\beta^0 = 1$ (solid line).

(*b*) At $\beta = \beta^0 = 1$ the model predicts a forward bifurcation into two symmetric branches of stable steady convection. These solutions correspond to either clockwise or counterclockwise flow. The experiments confirm these predictions, since, depending on the value of a small initial perturbation, a flow is established in one or the other direction. Repeated step-up procedures do not lead to a significantly higher probability for the occurrence of one or the other state of flow. The experimental data for the onset of convection during repeated runs lay within an interval bounded by two identical symbols □ in figure 15. Moreover, the measured steady mean velocities for each state of convection agree reasonably well with the calculated values. This holds also for the temperature distribution, represented by x_2 and x_3, as reported by Gorman *et al.* (1986) and Ehrhard (1988).

(*c*) A transition to time-dependent chaotic flow is predicted at the stability bounds β^* of the steady solutions. The corresponding experimentally determined values β^*_{exp} exceed the theoretical values of the model based on a constant heat transfer law with

$K = 0$. This can be seen in figure 15 by comparing the experimental data β^*_{exp} (symbols ○) with the theoretical values given by the curve of neutral stability $\beta^*(\alpha)$ (upper solid line). This has also been found by Gorman *et al.* (1986) in their experimental investigations. The data of these authors are also depicted in figure 15. Our theoretical analysis shows that a more realistic heat transfer law, equation (6), increases the critical heating rate β^* for the onset of time-dependent flow (see figure 4). For this reason we conclude that the implementation of the proposed heat transfer law (6) for the laminar flow regime (see in figure 8) improves the description of the actual flow and results in better agreement between theoretical and experimental data. We attribute the remaining discrepancies to an inaccuracy in the experimentally determined value $K \approx 0.35$. We have already determined in the theoretical analysis (see §2.5) that the stability bounds are extremely sensitive to this parameter K in the heat transfer law (6).

An increase of the critical heating rate β^* is similarly reported on theoretical grounds by Yorke *et al.* (1987). These authors find that by retaining radial diffusion terms in both momentum and heat transport equations, the solutions indicate a Hopf bifurcation at a considerably higher value of the heating rate. As the number of radial modes in their model is increased, they report convergence of the truncation. Thus the highest given mode ($N = 5$) should represent a good estimate of the location of the Hopf bifurcation and their figures read as $\beta^*(\alpha = 14) \approx 85$, $\beta^*(\alpha = 16) \approx 97$. These values are both far too high compared with our experimental findings. We conjecture that this discrepancy arises from the fact that, owing to the considerable curvature of the tube in our experiment, the velocity and temperature profiles in the cross-section A depart strongly from the axisymmetric shapes present in the model of Yorke *et al.* Thus their results need to be carefully interpreted when applied to a geometry with considerable curvature of the tube axis.

For values $\beta > \beta^*_{\mathrm{exp}}$ we find unsteady convection, as also reported by other authors (see e.g. Creveling *et al.* 1975; Gorman *et al.* 1986). According to the model equations, in the supercritical range, chaotic oscillations with intermittently growing amplitudes occur, resulting in repeated global flow reversals in the loop. In the moderate supercritical range of our experiments we observe irregular flow oscillations of limited amplitudes; however, no flow reversals occur in this range. Flow reversals are obtained in our experimental set-up without any external excitation only at very high supercritical heating rates. We ascribe this quantitative discrepancy between theory and experiment to the strong dissipative mixing effects caused by locally three-dimensional flow disturbances, including flow separation in the vicinity of the vertical parts of the test section. Such recirculating flow structures have also been reported by Damerell & Schoenhals (1979) and Stern & Greif (1987).

(*d*) The experiments confirm the existence of a range of subcritical instability of the steady convection. In this particular range a steady convection is permanent if external perturbations remain sufficiently small. For finite-amplitude disturbances, however, the system undergoes a transition to an oscillatory behaviour which affects all the variables of state. This behaviour may be of transient character, since the coexistence of a stable steady flow implies a finite probability for the system to return to a steady stable operation. In figure 15 the onset of a subcritical instability, as measured by Gorman *et al.* (1986) and as obtained in our experiments, is given by the symbols ●. For comparison the numerical results of Robbins (1977) are also plotted as a thin solid line which fits our own theoretical values β^{HO} (symbols ·) perfectly. It can be seen from figure 15 that all the experimental values exceed those obtained by calculations using the model equations.

(*e*) For a non-symmetrical arrangement of heat sources and sinks in the loop, the model equations predict an imperfect bifurcation of the steady solutions from the state without motion. The structure of this bifurcation is connected with the occurrence of one preferred steady convective flow which maintains stability up to higher heating rates compared with the symmetric case. The steady flow in the opposite direction has only a limited range of stability and is not connected to the origin of zero heating rate. Both features are confirmed by our experiments as shown in figure 13. Damerell & Schoenhals (1979) have likewise investigated these effects in their experiments. As far as the preferred state of flow originating from $\beta = 0$ is concerned the authors report corresponding observations, but, since detailed data were not given by these authors, a quantitative comparison with our results is not possible. Our experimental realization of the stable steady flow corresponding to the isolated branch of solutions is further strong support for the validity of the model equations (8). In this particular closed-loop geometry the isolated solution in the non-symmetric case has, to our knowledge, not been observed before. However, Bau & Torrance (1981) report a similar phenomenon in an asymmetrically heated open convection loop of rectangular form. Our theoretical results for the case of non-symmetric heating and cooling of the loop are in agreement with results reported by Hart (1984). Hart has performed an investigation of the model equations (8) with $\delta \neq 0$ and $K = 0$, and finds a continuous and an isolated branch of steady solutions. Using a linear perturbation analysis he obtains equivalent results for the stability of the steady solutions. As far as we know a detailed nonlinear bifurcation analysis of the model equations (8) for a non-symmetry parameter $\delta \neq 0$ has not previously been presented.

(*f*) Our calculations indicate that for increasing non-symmetry parameter δ the backward-directed bifurcation of the periodic solution at the Hopf point evolves continuously into a forward-directed one. This implies that a stable range of time-periodic flow exists for heating rates beyond the critical value β_2^*. We did not succeed in verifying this theoretical result in our experiments but the differences in the extension of the subcritical regions in our two non-symmetric experiments indicate that there is clear trend towards a smaller subcritical range when the non-symmetry angle δ is increased. We interpret this effect as an indication of the complete reversal of the direction of bifurcation of the periodic solution if an even stronger non-symmetry is imposed on the system.

The authors gratefully acknowledge helpful discussions with S. H. Davis, Northwestern University, and D. Riley, University of Bristol, during the course of this work. They also wish to thank Ch. Karcher, Kernforschungszentrum Karlsruhe, who was involved in the development of the numerical method, as well as W. Schneider and H. Streb, who contributed to this work while they performed their 'study thesis' and 'diploma thesis' at the Universität (TH) Karlsruhe.

REFERENCES

Bau, H. H. & Torrance, K. E. 1981 On the stability and flow reversal of an asymmetrically heated open convection loop. *J. Fluid Mech.* **106**, 417–433.

Creveling, H. F., De Paz, J. F., Baladi, J. Y. & Schoenhals, R. J. 1975 Stability characteristics of a single-phase convection loop. *J. Fluid Mech.* **67**, 65–84.

Damerell, P. S. & Schoenhals, R. J. 1979 Flow in a toroidal thermosyphon with angular displacement of heated and cooled sections. *Trans. ASME* C: *J. Heat Transfer* **101**, 672–676.

DAVIS, S. H. & ROPPO, M. N. 1987 Coupled Lorenz oscillators. *Physica D* **24**, 226–242.

EHRHARD, P. 1988 Dynamisches Verhalten der Naturkonvektion in geschlossenen Kreisläufen, Ph.D. thesis, Universität (TH) Karlsruhe; *KfK-Bericht* 4373.

EHRHARD, P., KARCHER, CH. & MÜLLER, U. 1989 Dynamical behaviour of natural convection in a double loop system. *Exp. Heat Transfer* **2**, 13–26.

FEIGENBAUM, M. J. 1980 Universal behaviour in nonlinear systems. *Los Alamos Science* (Summer issue), pp. 4–27.

GORMAN, M., WIDMANN, P. J. & ROBBINS, K. A. 1986 Non-linear dynamics of a convection loop: a quantitative comparison of experiment with theory. *Physica D* **19**, 255–267.

GREBOGI, C., OTT, E. & YORKE, J. A. 1982 Chaotic attractors in crisis. *Phys. Rev. Lett.* **48**, 1507–1510.

GREIF, R. 1988 Natural circulation loops. *Trans. ASME* C: *J. Heat Transfer* **110**, 1243–1258.

GUCKENHEIMER, J. & HOLMES, P. 1983 *Non-linear Oscillations, Dynamical Systems, and Bifurcations of Vector Fields*. Springer.

HART, J. E. 1984 A new analysis of the closed loop thermosyphon. *Intl J. Heat Mass Transfer* **27**, 125–136.

HOLODNIOK, M., KUBIČEK, M. & MAREK, M. 1982 Stable and unstable periodic solutions in the Lorenz model. *Techn. Universität München, Bericht TUM-M*8217.

HOPF, E. 1942 Abzweigung einer periodischen Lösung von einer stationären Lösung eines Differentialsystems. *Akad. d. Wiss. Leipzig, Berichte Math. Phys.* Kl. **94**.

JOSEPH, D. D. 1976 *Stability of Fluid Motions I*. Springer.

KUBIČEK, M. & MAREK, M. 1983 *Computational Methods in Bifurcation Theory and Dissipative Structures*. Springer.

LAVINE, A. S., GREIF, R. & HUMPHREY, J. A. C. 1987 A three-dimensional analysis of natural convection in a toroidal loop – the effect of Grashof number. *Intl J. Heat Mass Transfer* **30**, 251–262.

LORENZ, E. N. 1963 Deterministic non-periodic flow. *J. Atmos. Sci.* **20**, 130–141.

MALKUS, W. V. R. 1972 Non-periodic convection at high and low Prandtl numbers. *Mém. Soc. Royale de Sci. de Liège Ser.* 6, **4**, 125–128.

MCLAUGHLIN, J. B. & MARTIN, P. C. 1975 Transition to turbulence in a statistically stressed fluid system. *Phys. Rev.* A **12**, 186–203.

MERTOL, A. & GREIF, R. 1984 A review of natural circulation loops. *NATO Advanced Study Inst. of Natural Convection: Fundam. & Applic., Izmir*, pp. 1033–1081.

ROBBINS, K. A. 1977 A new approach to subcritical instability and turbulent transitions in a simple dynamo. *Math. Proc. Camb. Phil. Soc.* **82**, 309–325.

SCHLÜNDER, E. U. 1981 *Einführung in die Wärmeübertragung*. Vieweg, Braunschweig.

SPARROW, C. 1982 *The Lorenz equations: Bifurcations, Chaos and Strange Attractors*. Springer.

STERN, C. & GREIF, R. 1987 Measurements in a natural convection loop. *Wärme- & Stoffübertragung* **21**, 277–282.

WELANDER, P. 1967 On the oscillatory instability of a differentially heated fluid loop. *J. Fluid Mech.* **29**, 17–30.

WIDMANN, P. J., GORMAN, M. & ROBBINS, K. A. 1989 Nonlinear dynamics of a convection loop II: chaos in laminar and turbulent flows. *Physica D* **36**, 157–166.

YORKE, J. A. & YORKE, E. D. 1981 Chaotic behaviour and fluid dynamics. In *Hydrodynamic Instabilities and the Transition to Turbulence*. Topics in Applied Physics, vol. 45 (ed. H. L. Swinney & J. P. Gollup), pp. 77–95. Springer.

YORKE, J. A., YORKE, E. D. & MALLET-PARET, J. 1987 Lorenz-like chaos in a partial differential equation for a heated fluid loop. *Physica D* **24**, 279–291.

ZVIRIN, Y. 1981 A review of natural circulation loops in pressurized water reactors and other systems. *Nucl. Engng Design* **67**, 203–225.